

Global Stability Properties of the Climate: Melancholia States, Invariant Measures, and Phase Transitions

Valerio Lucarini^{1,2,3} and Tamás Bódai^{1,2}

¹*Centre for the Mathematics of Planet Earth, University of Reading, Reading, UK*

²*Department of Mathematics and Statistics, University of Reading, Reading UK*

³*CEN, University of Hamburg, Hamburg, Germany*

(Dated: November 29, 2021)

Abstract

For a wide range of values of the incoming solar radiation, the Earth features at least two attracting states, which correspond to competing climates. The warm climate is analogous to the present one; the snowball climate features global glaciation and conditions that can hardly support life forms. Paleoclimatic evidences suggest that in past our planet flipped between these two states. The main physical mechanism responsible for such instability is the ice-albedo feedback. In a previous work, we defined the Melancholia states that sit between the two climates. Such states are embedded in the boundaries between the two basins of attraction and feature extensive glaciation down to relatively low latitudes. Here, we explore the global stability properties of the system by introducing random perturbations as modulations to the intensity of the incoming solar radiation. We observe noise-induced transitions between the competing basins of attractions. In the weak noise limit, large deviation laws define the invariant measure and the statistics of escape times. By empirically constructing the instantons, we show that the Melancholia states are the gateways for the noise-induced transitions. In the region of multistability, in the zero-noise limit, the measure is supported only on one of the competing attractors. For low (high) values of the solar irradiance, the limit measure is the snowball (warm) climate. The changeover between the two regimes corresponds to a first order phase transition in the system. The framework we propose seems of general relevance for the study of complex multistable systems. At this regard, we relate our results to the debate around the prominence of contingency vs. convergence in biological evolution. Finally, we propose a new method for constructing Melancholia states from direct numerical simulations, thus bypassing the need to use the edge-tracking algorithm.

MSC Classification: 76U05 Rotating fluids; 82C26 Dynamic and nonequilibrium phase transitions (general); 60Gxx Stochastic processes; 37D45 Strange attractors, chaotic dynamics; 85A20 Planetary atmospheres; 76E20 Stability and instability of geophysical and astrophysical flows

I. INTRODUCTION

In the late 1960s and in the 1970s, Budyko, Sellers, and Ghil [1–3] proposed the idea that the Earth, in the current astrophysical and astronomical configuration, supports two co-existing attractors, the warm state we live in, and the so-called snowball state, characterised by global glaciation and globally averaged surface temperature of about 200-220 K. Using parsimonious yet physically meaningful energy balance models, they indicated that the bistability of the climate system is the result of the competition between the positive ice-albedo feedback (a glaciated surface reflects more effectively the incoming radiation) and the negative Boltzmann radiative feedback (a warmer surface emits more radiation to space). The relevance of the theoretical *ansatz* became apparent when paleoclimatic data showed that, indeed, our planet has been flipping in and out of states of global glaciations corresponding to the predicated Snowball states during the Proterozoic, about 650 Mya [4–6].

According to these energy balance models, the Earth’s climate is bistable for a substantial range of values of the solar irradiance S^* , which include the present day value. Below the critical value $S_{W \rightarrow SB}^*$, only the snowball state is permitted, whereas above the critical value $S_{SB \rightarrow W}^*$, only the warm state is permitted. Such critical values determining the boundaries of the region of bistability are defined by the occurrence of bifurcations that occur when, roughly speaking, the strength of the positive, destabilising feedbacks becomes as strong as the negative, stabilizing feedbacks. Indeed, models of different levels of complexity ranging up to the state-of-the-art Earth System Models currently used for climate projections agree on predicting the existence of multistability in the climate system and point to the fundamental mechanisms described above as responsible for it, as well as providing values for $S_{W \rightarrow SB}^*$ that are in broad agreement with those obtained using simple models [7–9]. We remark that the concentration of greenhouse gases - and the position of the continents have an impact on the values of $S_{W \rightarrow SB}^*$ and $S_{SB \rightarrow W}^*$ and on the properties of the warm and snowball states [10]. Extremely high values of the concentration of CO_2 seem to be needed to deglaciare from a snowball state [11].

Improving our understanding of the critical transitions associated to such a bistability is a key challenge of geosciences and has strong implications also in terms of the quest for understanding or anticipating planetary habitability. Planets in the habitable zone have astronomical and astrophysical configurations that allow, in principle, the presence of water at surface. Therefore, $S_{W \rightarrow SB}^*$ defines the cold boundary of the habitable zone. Clearly, an exoplanet in the habitable

zone can be in the regime of bistability: if the planet is in the snowball state, it will have very hard time supporting life¹. Additionally, astronomical parameters such as the obliquity of the planet [12, 13] or the length of the year [14] can have a dramatic effect on the properties of multistability of a planet in the habitable zone, up to the point of erasing it altogether. In particular, one expects that tidally locked planets with an active carbon cycle can never be found in a snowball state [15].

The dynamical landscape of the Earth's climate seems to be indeed richer than what is described above. Further investigations have proposed the possibility of the existence of alternative cold states with respect to the snowball one. Such states are characterised by the existence of a thin strip of ice-free region near the equator. Clearly, this possibility has key implications in terms of habitability and the evolution of life on Earth. Different physical mechanisms have been proposed for explaining the existence of such a state, based either on the role of a dynamical ocean [16] or the specific properties of the albedo of sea ice [17]. In fact, in a previous work [18] we have found that, indeed, a third co-existing stable state, intermediate between the snowball and the warm climate, can be found in a climate model featuring a very simplified representation of the oceanic heat transport, so that one might expect that a rich landscape multistability could be a more intrinsic property of the climate system. Additionally, the physics and the chemistry of the climate system features further complexities when one considers warmer conditions. For sufficiently large values of S^* , the warm state becomes unstable and the planet performs a transition to either the so-called moist greenhouse state or the so-called runaway greenhouse state (associated to massive evaporation of the oceans), which define the warm boundary of the habitable zone [19]; see discussions in [20, 21].

In what follows, we consider the simpler - yet extremely relevant - scenario where the only relevant co-existing climates are the snowball state and the warm state. As discussed in [9], the physics of the system is especially interesting when the critical transitions are approached. As the solar irradiance S^* nears the critical value $S_{W \rightarrow SB}^*$ with the system being in the warm state, the climatic engine becomes more efficient, because larger temperature gradients are realised inside the domain. Such an increased efficiency leads to a stronger atmospheric circulation, which is fuelled by temperature gradients and tends to reduce them by transporting heat from warm to cold regions, acting as a non-trivial diffusion process. Such a non-linear equilibration mechanism acts as a negative feedback and, broadly speaking, is a macroscopic manifestation of the second

¹ The project EDEN (<http://project-eden.space/>) combines ideas and methods in astrophysics, planetary sciences, and astrobiology to search for and characterize nearby habitable worlds.

law of thermodynamics. One of the results of the heat transport performed by the atmospheric circulation is the stabilization of the ice-line. When $S^* = S_{W \rightarrow SB}^*$, the ice-albedo feedbacks becomes as strong as the positive feedbacks of the system, and the system flips to snowball state with the ice-line reaching the equator. Similar mechanisms are in place when the system is in the snowball state and S^* nears, instead, $S_{SB \rightarrow W}^*$. When $S^* = S_{SB \rightarrow W}^*$, the ice begins to melt near the equator, leading to a rapid poleward retreat of the ice line.

One can rephrase the previous description by saying that at the critical transitions the climate system is not anymore able to dampen fluctuations due to (infinitesimal) external forcings. Using methods borrowed from the transfer operator theory [22], the investigation of the behaviour of the same model used in [9] has indeed shown that when S^* nears $S_{W \rightarrow SB}^*$, the spectral gap - defined as the distance between the subdominant Ruelle-Pollicott resonance [23, 24] and the unit circle - of the transfer operator constructed in a suitably defined reduced phase space vanishes. As a result, exponential decay of correlation is lost and the system experiences what is often referred to as *critical slowing down* [25]. We remark that, as discussed in [26], it is expected that the (near) closure of the spectral gap is associated to a very enhanced sensitivity of the system's statistics to perturbations. Specifically, a vanishing spectral gap leads to having a vanishing radius of expansion for the response theory describing how the measure of the system changes differentially with respect to small changes in the dynamics of the system [27].

A looming question is what lies in-between the stable co-existing climates within the region of bistability. Here, in simple models, it is often possible to identify unstable solutions sitting in-between the two stable climates. Such unstable solutions are, roughly speaking, ice-covered up to the mid-latitudes, and small perturbations applied to trajectories initialised on the edge states lead with probability one to the system falling eventually into either of the competing attractors [3, 28].

When studying more comprehensive climate models featuring chaotic dynamics, things are, as described in the next section, considerably more complex from a mathematical point of view, and the individuation of the unstable solutions is much harder. In a previous investigation [18], by taking advantage of the edge tracking algorithm presented in [29, 30] and there used to study the co-existence of a laminar attractor and long-lived turbulence in fluid mechanical set-ups, we have been able to find, for each value of S^* in the region of bistability, the *Melancholia* (M) states separating the two co-existing realisable warm and snowball climates.

As we shall see below, the M states are the natural extension of the saddle-type fixed points

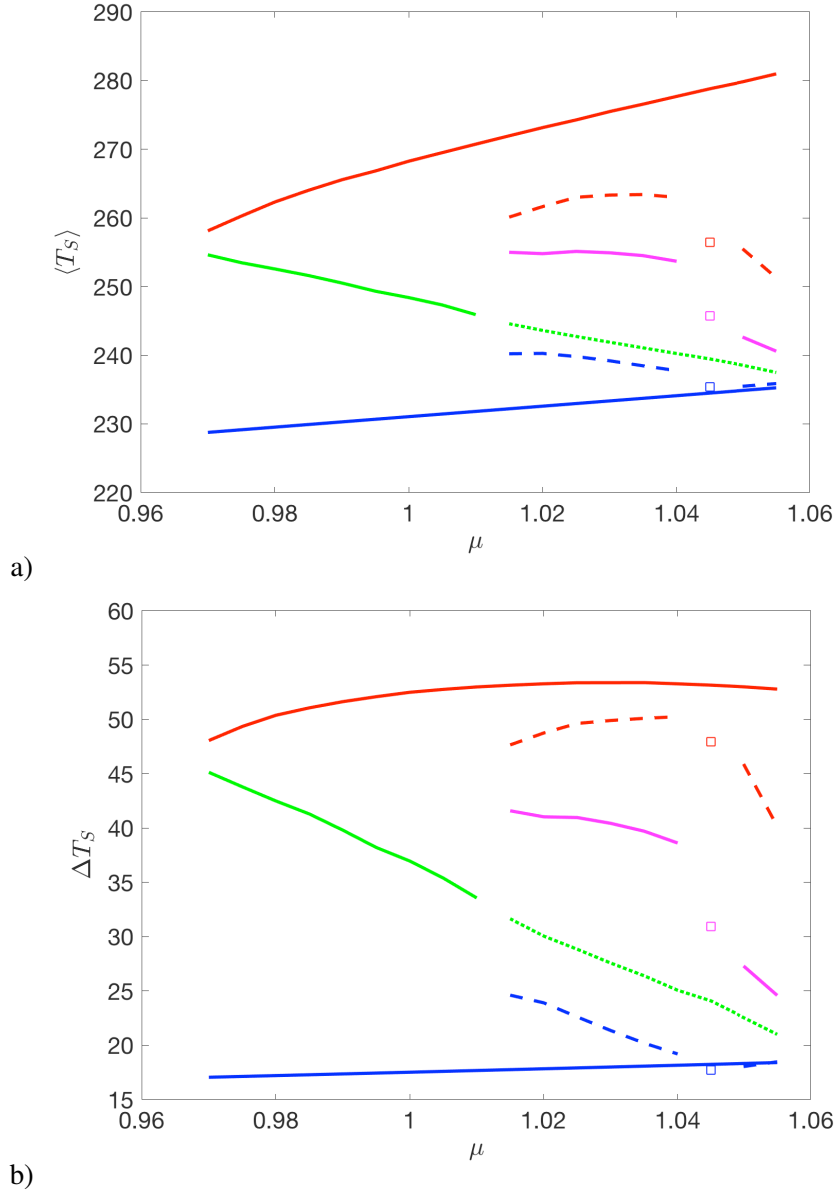


FIG. 1. Bifurcation diagram for the coupled climate model studied in [18]. Panel a) Globally averaged ocean temperature $\langle T_S \rangle$ vs μ . Bistability is found for a large range of values of μ . Red continuous line: warm attractor; blue continuous line: snowball attractor; green continuous line: chaotic M state; purple continuous line: mean properties of the symmetry broken chaotic M state; red dashed line: warm side of the symmetry broken chaotic M state; blue dashed line: cold side of the symmetry broken chaotic M state; green dotted line; transient symmetric chaotic M state; empty squares: warm side (red), cold side (blue) and average properties of the third attractor. The warm-to-snowball tipping point is located at $\mu \sim 0.965$; the snowball-to-warm tipping point is located at $\mu \sim 1.055$; See [18].

found in dynamical systems living in energy landscapes to the case where more general dynamics is considered [31–34]. The M states are embedded in the boundary between the two basins of attraction. The analysis was performed using an intermediate complexity climate model with $O(10^4)$ degrees of freedom. Figures 1a)-b) summarize the main properties of the system, by showing the long term averages of the globally averaged surface temperature $\langle T_S \rangle$ and of the temperature difference between low and high latitudes ΔT_S as a function of the relative solar irradiance $\mu = S^*/S_0^*$, where S_0^* is the present day value. By focusing on the M states we have been able to show the existence of much richer than previously thought dynamical landscape.

The properties of the M states are non-trivial. Up to $\mu \sim 1.01$, the M state is chaotic and is characterised by longitudinal symmetry in its statistical properties, just as the boundary conditions of the system, are, indeed, longitudinally symmetric. The chaotic dynamics manifests itself as weather variability in form not too dissimilar from the usual one observed in stable climates. Nonetheless, on long time scales, orbits initialised near the M states drift to either the warm or the cold snowball state, as a result of the positive ice-albedo feedback. For $\mu \sim 1.01$, we observed that the symmetric M state becomes transient, evolving very slowly (on a time scale much longer than the other ones typical of the system) into a symmetry-broken state, where very cold and very warm conditions co-exist, separated by two regions of very strong *longitudinal* temperature gradient. The two regions feature rather different dynamical behaviour and the boundary between them rotates very slowly in time. The nontrivial bifurcation associated to such a symmetry break leads to a dynamical regimes that resembles *chimera states* in extensive systems [35, 36]. The third climate state mentioned before exists in a small parametric window near $\mu \sim 1.045$ [18].

We remark that the dynamical systems viewpoint clarifies that the critical transitions for the warm (snowball) state occurring when S^* approaches the critical value $S_{W \rightarrow SB}^*$ ($S_{SB \rightarrow W}^*$) are associated to the collision between the edge state and one of the warm (snowball) climates, according to the dynamical scenario of boundary crisis [33]. The system’s reduced ability to dampen fluctuations near the tipping points and the associated shrinking of the spectral gap described above can be seen, dynamically, as the result of the fact that the attractor *attracts less effectively* orbits in its immediate neighbourhood because of the presence of a nearby edge state state. See a discussion of this specific point in [25].

A. This Paper: Goals and Main Results

Studying multistable systems in general, and the climate system in particular, using deterministic autonomous dynamical systems faces two important limitations, both resulting from the fact that the phase space is partitioned into disjoint invariant sets - the various basins of attractions and their respective boundaries. First, it is not possible to account for transitions between the co-existing basins of attraction. Instead, transitions between distinct *regimes of motion* are observed in many systems of interest. Additionally, one cannot establish an ergodic, physically relevant invariant measure, as the co-existing attractors are disjoint and one cannot assign a weight to each of them. Hence, one cannot answer the question of how likely it is for the system of interest to be found at a given time in a specific regimes of motion. Instead, all the statistical properties of an orbit are conditional on which invariant set its initial conditions belong to. Indeed, building upon the preliminary results reported in a short communication [37] and giving them much broader scope, we want to address these relevant aspects that cannot be treated taking the viewpoint of autonomous deterministic dynamics.

For the benefit of the reader, we report below the main goals of our investigation and the main findings presented in this paper.

We will introduce a stochastic forcing to the model studied in [18] as a Gaussian perturbation with variance σ^2 modulating the intensity of the incoming solar radiation. This impacts the radiative budget of the planet in a very nontrivial way and, thanks to the ice-albedo feedback, acts as a multiplicative noise. Additionally, we conjecture, supported by physical arguments, that the combination noise and deterministic dynamics lead to a hypoelliptic diffusion process, i.e. the noise propagates to all degrees of freedom of the system [38]. The presence of a random forcing allows the system to perform transitions between the neighbourhoods of the deterministic attractors, crossing the basin boundaries that, in the unperturbed case, are impenetrable; see some classical results in [39–41]. The consideration of a random forcing will allow us to construct the ergodic invariant measure of the system by performing long integrations, and investigate the properties of noise-induced transitions.

Following [34, 42–44], we will propose that, in the weak noise limit, the invariant measure can be written as a large deviation law with the following notable properties. The relevant exponent is proportional to minus a pseudo-potential function divided by $\sigma^2/2$. In the region of bistability, the pseudo-potential has local extrema associated to the attractors (local minima) and the M states (lo-

cal maxima) of the deterministic system. In the region where only one stable state is realised in the deterministic case, the pseudo-potential has just one local (and global) minimum, corresponding to the unique attractor.

As a result, in the case of multistability, the logarithm of the average permanence time in a basin of attraction is approximately given, apart from an additive constant, by the product of $2/\sigma^2$ times the difference between the value of the pseudo-potential at the M state through which the transitions takes place and its value at the corresponding attractor. We also show that the stochastically averaged exit trajectories connect the attractor with the M state, which is indeed the most likely exit point from the deterministic basin of attraction. In the weak noise limit, such paths correspond to the instantons. These can be defined as minimizers of a the Freidlin-Wentzell action [40, 41, 45, 46]. In our simulations, we show that such an identification becomes more accurate as the intensity of the noise is decreased. Exploiting this property, we also propose a new general method for constructing the M states via direct numerical integration of stochastic differential equations, thus bypassing the need to resort to the edge tracking algorithm mentioned above.

Evaluating the average permanence times in some selected experiments allows us to reconstruct the properties of the described pseudo-potential in a very high-dimensional system, and to predict how the populations of the regions nearby the two deterministic attractors change as a function of the intensity of the noise. In particular, we discover that, since generally the local minima of the pseudo-potential corresponding to the two attractors have different values, in the zero-noise limit only one attractor - the one corresponding to the global minimum of the pseudo-potential - is populated. Nonetheless, an individual trajectory may in fact persist near the competing metastable state for a very long time, as the permanence time in the corresponding basin of attraction also diverges (but at a slower rate than for the asymptotic state).

As indicated by intuition, for low values of S^* , the noise selects as limit measure the snowball state, while for high values of S^* , the limit measure is the warm attractor. The changeover takes place for a critical value of $S^* = \mu_{crit}S_0^*$, where S_0^* is the present solar irradiance, and $\mu_{crit} \approx 1.005$. For this value of S^* , the equivalent of a first order phase transition for equilibrium systems takes place in the system. The order parameter that more obviously captures the transition is the globally averaged surface temperature.

As discussed later in the conclusions, the specific findings reported here suggest general ideas about how to study multistable complex systems and how to define their global stability proper-

ties. Additionally, we show how the framework presented in the paper is potentially suitable for clarifying the role played in complex historical processes by *contingency*, as discussed by Gould [47] in the context of evolutionary biology.

The paper is structured as follows. In Section II we summarise the main mathematical concepts and ideas we have used to frame our investigation, to perform the data analysis, and to interpret our results. In Section III we report the modelling suite we have used, describe the data we have produced, and give information on how they have been processed. In Section IV we present and discuss our results. In Section V we summarize and interpret our findings, describe the limitations of our work, and propose ideas for future investigations. In Appendix A we propose and test numerically a new method for constructing the M states by looking at the intersections of instantons constructed by taking into account three different noise laws superimposed to the same deterministic dynamics.

II. MATHEMATICAL BACKGROUND

A. Geometry of the Phase Space: Attractors and Edge States

The investigation of systems possessing multiple steady states is an extremely active area of interdisciplinary research, encompassing mathematics, natural sciences, and social sciences. The recent review by Feudel et al. [48], introducing a special issue on the topic, gives a rather complete overview of the state-of-the-art of the ongoing activities on this topic and provides several interesting examples. In the context of Earth sciences, it is more common to refer to critical transitions in multistable systems using the expression *tipping points*, which has received a great popularity following a paper by Lenton *et al.* [49].

A possible way to introduce the mathematical background for multistable systems is the following. We consider a smooth autonomous continuous-time deterministic dynamical system defined on a smooth finite-dimensional compact manifold \mathcal{M} (in what follows, a subset of \mathbb{R}^N). The orbit evolves from an initial condition $\mathbf{x}_0 \in \mathcal{M}$ at time $t = 0$. We define $\mathbf{x}(t, \mathbf{x}_0) = S^t(\mathbf{x}_0)$ as the orbit at a generic time t , where S^t indicates the evolution operator. The corresponding set of ordinary differential equations are:

$$\dot{\mathbf{x}}(t) = \mathbf{F}(\mathbf{x}(t)) \tag{1}$$

where $\mathbf{F}(\mathbf{x}(t)) = d/d\tau S^\tau(\mathbf{x}(t))|_{\tau=0}$ is a smooth N -dimensional vector field. We define such a

dynamical system as multistable if it features more than one asymptotic states. Specifically, we mean that one can define two or more attractors Ω_j , $j = 1, \dots, J$ with finite Lebesgue measure basin of attraction. Each of the attractors is an invariant set and is the support of an invariant measure of the system. The asymptotic state where the trajectory falls into is determined by its initial conditions, and the phase space is partitioned between the basins of attraction B_l of the various attractors Ω_j and the boundaries ∂B_l , $l = 1, \dots, L$ of such basins. We assume, for simplicity, that within each basin of attraction an ergodic measure can be defined as the limit of the empirical measure constructed by averaging over infinitely long forward trajectories almost everywhere with respect to Lebesgue in the initial conditions. In other terms, all the invariant measures of the system can be written as a convex sum of its $j = 1, \dots, J$ ergodic components, each supported on the corresponding attractor Ω_j , $j = 1, \dots, J$.

Let us for the moment assume that the dynamics is determined by an energy landscape defined by the smooth potential $U(\mathbf{x})$, so that $\mathbf{F}(\mathbf{x}) = -\nabla U(\mathbf{x})$. Therefore, one has that $\dot{U}(\mathbf{x}) = -|\nabla U(\mathbf{x})|^2$ (U being a Lyapunov function), which leads to identifying the attractors with the local minima \mathbf{x}_j , $j = 1, \dots, J$ of the potential $U(\mathbf{x})$, which are invariant sets [50]. Using the classic geographical metaphor responsible for the use of the word *basin*, the basin of attraction of the lake \mathbf{x}_j corresponds to its watershed, or precipitation catchment area, where $U(\mathbf{x})$ is the orography. Additionally, the basin boundaries are the mountain crests, which are manifolds of co-dimension one, while the mountain passes are the saddles Π_l , $l = 1, \dots, L$ situated between the attractors contained in the basin boundaries. The saddles are invariant sets and are, globally speaking, repellers, but can be thought of as relative attractors because they attract the orbits whose initial conditions are exactly on the basin boundaries (which have zero Lebesgue measure).

The geometry of the phase space becomes much more interesting when the dynamics is more complex than in the case of an energy landscape [31–33, 51]. One can be in the situation where the asymptotic dynamics on one or more of the competing attractors can be chaotic (meaning here that at least one Lyapunov exponent is positive and unstable periodic orbits are dense). Additionally, in some systems, chaotic dynamics can be realised on one or more of the saddles embedded in the basin boundaries. Therefore, as opposed to the energy landscape case, saddles can be non-trivial geometrical objects being the support of a possibly nontrivial measure. While typically one is interested in the asymptotic states of a complex multistable system, the properties of the basin boundaries and of the possibly chaotic saddles is extremely relevant because it is key for understanding the global stability properties of the system and for interpreting its critical transitions. A

very relevant example can be found in the well-known case of boundary crisis, where the critical transition takes place when, for a given value of a parameter, one attractor and one saddle collide, thus leading to the disappearance of one asymptotic state [33].

A fascinating aspect of multistable systems is the following. If the first Lyapunov exponent of a chaotic saddle is larger than the inverse of the life time of the saddle state itself (which measures the rate at which orbits initialised near the saddle state are repelled towards the two nearby asymptotic states), then the basin boundary separating the basin of attraction of the two asymptotic sets has co-dimension strictly smaller than one. In two-dimensional maps, it has been proved that in this case the basin boundary is not a manifold, but rather a *rough fractal* [31, 34, 51]. In [18], despite high-dimensionality of the system, one could detect that the co-dimension of the basin boundary is strictly smaller than one. In fact, such co-dimension was found to be very close to zero, as a result of time scale difference between the most relevant instabilities: the climatic instability due to the ice-albedo feedback acting near the M state is much slower than the fast weather-like instability associated to baroclinic processes occurring on the M state. This implies that near the basin boundary there is basically no predictability of the second kind in the sense of Lorenz [52]. The basin boundary is, *de facto*, a grey zone, and we can hardly assess where orbits initialised near the boundary will asymptotically end up.

B. Impact of Stochastic Perturbations: Invariant Measure and Noise-induced Transitions

The goal of our investigation is to analyse the impact of imposing a random forcing on the deterministic dynamics discussed above. Specifically, for a given choice of noise law and strength, we want to construct the invariant measure of the system, which allows us to understand whether, for a given value of the solar irradiance, the warm climate or the snowball climate is more likely to be realised. We also want to be able to study the statistics of the noise-induced transitions, and to understand the role played by the edge states in channeling the transitions. Processes that can be described as a noise-induced escape from an attractor have long been studied in the natural sciences; see [39–41].

Let's consider the following stochastic differential equation in the Itô form:

$$d\mathbf{x}(t) = \mathbf{F}(\mathbf{x}(t))dt + \sigma \mathbf{s}(\mathbf{x})d\mathbf{W} \quad (2)$$

where $\dot{\mathbf{x}}(t) = \mathbf{F}(\mathbf{x}(t))$ is a vector flow - drift term - with multiple steady states as in Eq. 1,

$d\mathbf{W}$ is an M -dimensional Brownian motion, and the matrix $\mathbf{s}(\mathbf{x}) \in \mathbb{R}^{N \times M}$ - volatility - is such that $\mathbf{s}(\mathbf{x})^T \mathbf{s}(\mathbf{x})$ is the covariance matrix of the noise. Finally, $\sigma \geq 0$ is a bookkeeping parameter controlling the intensity of the noise. In what follows, we draw from the classical Freidlin-Wentzell [42] theory and from the more recent extensions able to address the case of chaotic dynamics in the deterministic case of $\sigma = 0$ [34, 43, 44].

We first need to assume that we are considering a hypoelliptic diffusion process: while the covariance matrix of noise can be singular, a smooth invariant density with respect to Lebesgue is realised because the noise is propagated to all the coordinates through the drift term. Technically, this is realised if the drift term F and the columns of the matrix s satisfy the so-called Hörmander condition, *i.e.* the Lie algebra generated by them has dimension N everywhere; see for instance [38]². We then assume that either the noise law is additive ($\mathbf{s}(\mathbf{x})$ is a constant) or multiplicative in a very mild sense, meaning (see also [53, 54]) that $\mathbf{s}(\mathbf{x})$ undergoes just a weak modulation in the phase space, so that one observes no new stable states that have no deterministic counterpart as a result of adding noise [55]. Then, in the weak noise limit given by $\sigma \rightarrow 0$, the invariant measure $W_\sigma(\mathbf{x})$ of the system can be written as a large deviation law:

$$W_\sigma(\mathbf{x}) \approx Z(\mathbf{x}) \exp\left(-\frac{2\Phi(\mathbf{x})}{\sigma^2}\right), \quad (3)$$

where $Z(\mathbf{x})$ is a prefactor and $\Phi(\mathbf{x})$ is the pseudo-potential.

For a given deterministic vector flow $\mathbf{F}(\mathbf{x}(t))$, different choices of the noise law will lead to different invariant densities: in Eq. 3, both the prefactor $Z(\mathbf{x})$, and more decisively, the pseudo-potential $\Phi(\mathbf{x})$ depend on the choice of $\mathbf{s}(\mathbf{x})$. Note that $\Phi(\mathbf{x}) = U(\mathbf{x})$ if $\mathbf{s}(\mathbf{x})^T \mathbf{s}(\mathbf{x}) = \mathbf{1} \in \mathbb{R}^{N \times N}$ and the deterministic vector field can be written as $\mathbf{F}(\mathbf{x}) = -\nabla U(\mathbf{x})$.

One can establish general properties for the pseudo-potential $\Phi(\mathbf{x})$ that apply to all choices of noise laws, and, once a noise law is chosen, derive how the properties of the system change as a function of the parameter σ . In general, one has that, regardless of the noise law, $\Phi(\mathbf{x})$ has local minima supported on the attractors Ω_j , $j = 1, \dots, J$ of the deterministic dynamics. Additionally, $\Phi(\mathbf{x})$ has a constant value on the support of each M state and of each attractor, respectively. We remark that such sets can be strange and, as discussed before, support chaotic dynamics [43, 44].

Unless degeneracies are present, the probability that a noisy trajectory with initial condition in

² Assuming an elliptic diffusion process is extremely restrictive because it requires all coordinates to be driven by Gaussian noise.

the basin of attraction of Ω_j does not escape it over a time span of length p decays exponentially:

$$P(p) = \frac{A(p)}{\bar{\tau}_\sigma} \exp\left(-\frac{p}{\bar{\tau}_\sigma}\right). \quad (4)$$

where we have included the possibility of a pre-factor. The expression for the expected escape time is:

$$\bar{\tau}_\sigma \propto \exp\left(\frac{2(\Phi(\Pi_l) - \Phi(\Omega_j))}{\sigma^2}\right), \quad (5)$$

where $\Delta\Phi = \Phi(\Pi_l) - \Phi(\Omega_j)$ is the potential barrier height, constructed as proportional to the difference between the lowest among the values of the pseudo-potential evaluated at the M states surrounding Ω_j (let's refer to this M state as Π_l) and the value of the pseudo-potential on the attractor Ω_j) [34]. Note that Eq. 5 is a generalisation of the classic Kramers' formula [56].

In the weak-noise limit, the transition paths are exponentially more likely to follow specific paths in the phase space. Such paths are called instantons and can be constructed as minimizers of the related Freidlin-Wentzell action [40, 41, 45, 46]. In general, different choices of the noise law will lead to different instantons, as the specific form of $\mathbf{s}(\mathbf{x})$ enters in the definition of the action. Nonetheless, under the hypotheses stated above on the noise laws, instantons corresponding to different choices of $\mathbf{s}(\mathbf{x})$ share some essential qualitative properties: they connect a point on the attractor Ω_j to a point in the neighbouring M state Π_l where the pseudo-potential has the lowest value. We remark that if the attractors and the M states are more complex sets than isolated points, the instantons connecting them are not unique, because in principle any point in the attractor can be linked by an instanton to any point in the M state), as a result of the fact that the pseudo-potential is constant on Ω_j and Π_l . We conclude that the M states are the gateways for the noise-induced escapes from the deterministic basins of attraction, and generalise the saddle points discussed above in the case of dynamics taking place in an energy landscape (which is the case described by the Kramers' formula [56]).

See Appendix A for a discussion of how to construct the M states of a system by studying the intersection of instantons constructed according to different noise laws acting on the same deterministic dynamics, and considering the weak noise limit. Such a method seems novel and is alternative to the edge tracking algorithm mentioned above.

Let's now take the simpler case of bistable systems, where we have two attractors Ω_1, Ω_2 , and

one edge state Π_1 . We can then write transition times as follows:

$$\tau_\sigma^{1 \rightarrow 2} \propto \exp\left(\frac{2(\Phi(\Pi_1) - \Phi(\Omega_1))}{\sigma^2}\right) \quad (6)$$

$$\tau_\sigma^{2 \rightarrow 1} \propto \exp\left(\frac{2(\Phi(\Pi_1) - \Phi(\Omega_2))}{\sigma^2}\right) \quad (7)$$

where we have that

$$\frac{\tau_\sigma^{1 \rightarrow 2}}{\tau_\sigma^{2 \rightarrow 1}} \propto \exp\left(\frac{2(\Phi(\Omega_2) - \Phi(\Omega_1))}{\sigma^2}\right), \quad (8)$$

which implies that, in the weak noise limit, both escape times diverge, but the escape time out of the attractor corresponding to the lower value of the pseudo-potential diverges faster. Note that one can expect the proportionality constant in Eq. 8 to be $O(1)$. Taking a maximally coarse-grained view on the problem, where we consider the state as represented by the populations $P_{1,\sigma}$, $P_{2,\sigma}$ of the neighbourhood of the two attractors, we can write the following master equation:

$$\dot{P}_{1,\sigma} = -\frac{P_{1,\sigma}}{\tau_\sigma^{1 \rightarrow 2}} + \frac{P_{2,\sigma}}{\tau_\sigma^{2 \rightarrow 1}} \quad (9)$$

$$\dot{P}_{2,\sigma} = -\frac{P_{2,\sigma}}{\tau_\sigma^{2 \rightarrow 1}} + \frac{P_{1,\sigma}}{\tau_\sigma^{1 \rightarrow 2}}. \quad (10)$$

At steady state, we obtain that

$$\frac{P_{1,\sigma}}{P_{2,\sigma}} = \frac{\tau_\sigma^{1 \rightarrow 2}}{\tau_\sigma^{2 \rightarrow 1}} \propto \exp\left(\frac{2(\Phi(\Omega_2) - \Phi(\Omega_1))}{\sigma^2}\right). \quad (11)$$

We remark that one could obtain the same results regarding the ration of the populations by integrating the invariant measure given in Eq. 3 in the neighborhood of the attractors and taking a saddle point approximation. The previous equation implies that in the weak-noise limit only one of the two deterministic attractors will be populated, and specifically the one where the pseudo-potential has lower value. We remark that two different noise laws, which define two different pseudo-potentials, will feature different properties for the transition rates between the two basins of attraction and might determine a different selection of the dominating population in the weak noise limit. One can easily extend the master equation defined above to the case where multiple states and multiple paths of transitions are present.

III. NUMERICAL MODELLING

The climate model considered here is constructed by coupling the primitive equations atmospheric model PUMA [57] with the Ghil-Sellers energy balance model [3], the latter describing

succinctly the meridional oceanic heat transport. It has been already presented in [18] with the name of PUMA-GS, but we report here again its formulation in order to elucidate the role of stochastic forcing, which was absent in the previous version. The stochastic forcing is added as a fluctuating term modulating the value of the incoming radiation determining the energy input into the system.

A. The Atmospheric Component

The atmospheric component of the PUMA-GS model is provided by PUMA [57], which consists of a dynamical core: the dry hydrostatic primitive equations on the sphere (mapped laterally by the latitude ϕ and longitude λ), solved by a spectral transform method (only linear terms are evaluated in the spectral domain, nonlinear terms are evaluated in grid-point space). The equations for the prognostic state variables, the vertical component (with respect to the local surface) of the absolute vorticity $\zeta = \xi + 2\nu\Omega_E$ (where ξ is the vertical component of the relative vorticity, $\nu = \sin \phi$, and $\Omega_E = 2\pi/\text{day}$ is the angular frequency of the Earth rotation) the (horizontal) divergence of the velocity field D , the (atmospheric) temperature $T_a = \bar{T}_a + T'_a$ (separated into a time-independent arbitrary reference part \bar{T}_a and anomalies T'_a), and the logarithmic pressure (normalized by the surface pressure p_s) $\sigma = \ln p/p_s$, read as follows:

$$\partial_t \zeta = s^2 \partial_\lambda F_v - \partial_\nu F_u - \tau_f^{-1} \xi - K \nabla^8 \xi, \quad (12)$$

$$\begin{aligned} \partial_t D = s^2 \partial_\lambda F_u + \partial_\nu F_v - \nabla^2 [s^2 (U^2 + V^2)/2 + \Phi + T_a \ln p_s] \\ - \tau_f^{-1} D - K \nabla^8 D, \end{aligned} \quad (13)$$

$$\begin{aligned} \partial_t T'_a = s^2 \partial_\lambda (U T'_a) - \partial_\nu (V T'_a) + D T'_a - \dot{\sigma} \partial_\sigma T_a \\ + \kappa T_a \omega / p + \tau_c^{-1} (T_R(T_S) - T_a) - K \nabla^8 T'_a, \end{aligned} \quad (14)$$

$$\partial_t \ln p_s = -s^2 \partial_\lambda \ln p_s - V \partial_\nu \ln p_s - D - \partial_\sigma \dot{\sigma}, \quad (15)$$

$$\partial_{\ln \sigma} \Phi = -T_a, \quad (16)$$

where $s^2 = 1/(1 - \nu^2)$, $F_u = V\zeta - \dot{\sigma} \partial_\sigma U - T'_a \partial_\lambda \ln p_s$, $F_v = -U\zeta - \dot{\sigma} \partial_\sigma V - T'_a s^{-2} \partial_\nu \ln p_s$, $U = u \cos \phi$, $V = v \cos \phi$, u , v being respectively the horizontal and vertical wind velocity components, and Φ is the geopotential height. Equations 12,13, and 15 express the conservation of momentum, Eq. 14 expresses the conservation of energy, and Eq. 16 is the equation of state.

A number of simple parametrizations are adopted in order to improve the realism and the stability of the model. Firstly, the hyperdiffusion operator $K \nabla^8$ is added to the equations of vorticity,

divergence and temperature, to represent *subgrid-scale* eddies. Secondly, *large-scale* dissipation of vorticity and divergence is facilitated by Rayleigh friction of time scale τ_f . Thirdly, the physics of diabatic heating due to radiative heat transport is parametrized by Newtonian cooling: the temperature field is relaxed (with a time scale τ_c) towards a reference or *restoration* temperature field T_R , which can be considered a radiative-convective equilibrium solution. We adopt the following simple expression for the restoration temperature [57]:

$$T_R = (T_R)_{tp} + \sqrt{[L(z_{tp} - z(\sigma))/2]^2 + S^2} + L(z_{tp} - z(\sigma))/2, \quad (17)$$

$$(T_R)_{tp} = \langle T_S \rangle - \bar{L}z_{tp}, \quad (18)$$

$$L(\lambda, \phi) = \partial_z T_R = (T_S(\lambda, \phi) - (T_R)_{tp})/z_{tp}, \quad (19)$$

where $(T_R)_{tp}$ and z_{tp} are the temperature and height of the tropopause, respectively, L (\bar{L}) is the (average) lapse rate, $\langle T_S \rangle$ is the globally averaged surface temperature, and $z(\sigma)$ is determined by an iterative procedure [57]. The above expressions indicate that the restoration temperature profile is *anchored* to the surface temperature T_S . However, as Eq. 18 indicates, T_R at any one point on the sphere is determined by not only the local (dynamical) surface temperature, but also the global average $\langle T_S \rangle$. We note that $T_a(\sigma = 1)$ is obtained by linear extrapolation, according to $T_a(\sigma = 1) \approx T_a(\sigma = 0.9) + \eta(T_S - T_R(\sigma = 0.9))$, $0 < \eta < 1$. With $\eta = 1$ the coupling term is $k_3(T_a(\sigma = 1) - T_S) \approx k_3(T_a(\sigma = 0.9) - T_R(\sigma = 0.9))$. Generally $\overline{T_a(\sigma = 1)} - \overline{T_S} \neq 0$ (laterally inhomogeneous heating), but $\overline{\langle T_a(\sigma = 1) \rangle} = \overline{\langle T_S \rangle}$, where the overbar denotes averaging with respect to time.

For our setup we choose: $K^{-1} = 0.25$ days, $\tau_c = 30$ days, $\tau_f = 1$ day. $\bar{L} = 0.0065$ K/m, $z_{tp} = 12000$ m, and $k_3 = 10^{-4}$. We also adopt a coarse resolution of T21 (i.e., the series of spherical harmonics are triangular-truncated at total wave number 21). This implies the optimal number of Gaussian grid points: $N_{lon} = 2N_{lat} = 64$. Finally, we consider $N_{lev} = 10$ vertical layers and consider a vanishing orography, so that we have a zonally-symmetric configuration. The equations are integrated numerically using a $\Delta t = 1$ [hour] time step size.

B. The Ocean Component and the Stochastic Forcing

The surface temperature T_S is taken to be governed by the a 2D version of the GS EBM [3, 28]. This model includes a simple yet effective representation of the ice-albedo feedback, and basically defines the slow manifold of the coupled atmosphere-ocean system. The partial differential equa-

tion describing the evolution of the ocean surface temperature field $T_S = T_S(t, \phi, \lambda)$ is written as:

$$\partial_t T_S(t, \phi, \lambda) = \mu \frac{I(\phi) S_0^*}{C(\phi)} \frac{1}{4} (1 - \alpha(\phi, T_S)) - \frac{O(T_S)}{C(\phi)} - \frac{D_\phi[T_S]}{C(\phi)} + \frac{\chi[T_S, T_A]}{C(\phi)} + s.f., \quad (20)$$

where S_0^* is the present solar irradiance (the factor 4 emerges looking at the geometry of the Earth-Sun system (see [58]), $\mu = S^*/S_0^*$ as introduced in Sect. I, while the heat capacity $C(\phi)$ and the geometrical factor $I(\phi)$ are explicitly dependent on ϕ only, thus enforcing zonally-symmetric boundary conditions. The albedo α depends on ϕ and, critically, on T_S , with a rapid transition from strong albedo for low values of T_S ($\alpha_{max} = 0.6$) to weak albedo for $T_S \gtrsim 260$ K ($\alpha_{min} = 0.2$), which fuels the positive ice-albedo feedback. Additionally, O is the outgoing radiation per unit area, expressed as a monotonically increasing function of T_S (this is responsible for the negative Boltzmann feedback, taking into account also the greenhouse effect), D is a diffusion (taking place only along the meridional direction) operator parametrizing the meridional heat transport, and χ describes the heat exchange with the atmosphere. See [18, 28] for further details.

Finally, the last term represents the stochastic forcing, which is introduced as a random modulation of incoming solar radiation, so that we have:

$$s.f. = \sigma s(T_S, \phi, \lambda) \frac{dW}{dt} = \sigma \mu \frac{I(\phi) S_0^*}{C(\phi)} \frac{1}{4} (1 - \alpha(\phi, T_S)) \frac{dW}{dt} \quad (21)$$

where σ controls the intensity of the noise, s defines the noise law, and dW is the increment of a one-dimensional Wiener process. Since s depends explicitly on T_S via the term $\alpha(\phi, T_S)$, we are dealing with a multiplicative noise law. We consider the Itô convention for noise. Adding a Gaussian random variable of variance σ at each time step Δt (1 hour) of the model amounts to considering that, on the time scale $\tau = N \times \Delta t$, the relative fluctuation of the solar irradiance is $\sigma_\tau = \sigma/\sqrt{N}$.

C. Remarks

We briefly discuss how reasonable it is to expect that the properties of the system under consideration can be explained using the theoretical framework presented in Section II.

Assuming the validity of the hypoellipticity condition, as done in Sect. II B, amounts to saying, in this specific case, that the stochastic forcing acting on the oceanic surface temperature - see Eqs. 20-21 - propagates to all degrees of freedom of the coupled system thanks to the interplay

between stochastic and deterministic components of the dynamics. On physical grounds, such an assumption seems convincing if one considers that the ocean surface temperature drives the restoration profile of the atmospheric temperature - see Eq. 17 - and that fluctuations of such a profile modulate the atmospheric instabilities, whose energy cascades down to the smallest scales resolved by the model; see [59, 60] for a detailed treatment of the energetics of the climate system.

A second critical point is that we are considering a multiplicative noise law. Nonetheless, our dispersion matrix, encoded by the factor $1 - \alpha(\phi, T_S)$ - see Eq. 21 - has a smooth dependence on the variable T_S . Additionally, the factor $1 - \alpha(\phi, T_S)$ is bounded in the phase space between 0.4 ($\alpha = \alpha_{max} = 0.6$, ice-cover) and 0.8 ($\alpha = \alpha_{min} = 0.2$, very warm conditions with the absence of ice cover). Therefore, we are confident that our noise law obeys the mathematical conditions indicated in [34, 43, 44, 53, 54] for the results contained in Section II to hold.

We can also provide a more physical interpretation of why the multiplicative noise we are considering should allow for the emergence of the large deviation laws described in Section II. In the phase space region near the cold attractor, we have that $1 - \alpha(\phi, T_S) \sim 0.4$ since the temperature T_S is extremely low and the planet is fully glaciated (or almost entirely so), so that $\alpha(\phi, T_S)$ is virtually constant, with $\alpha(\phi, T_S) \sim \alpha_{min}$. Near the warm attractor, the properties of the field $\alpha(\phi, T_S)$ are slightly more complex, because part of the planet is glaciated and part of it is ice-free. Our working hypothesis is that, to a first approximation, the stochastic forcing we have introduced can be treated as corresponding to perturbing the system with additive noise of different strengths near the cold and warm attractors, plus a transition region between the two attractors, where the effective intensity of the noise decreases with the globally averaged surface temperature $\langle T_S \rangle$ and the multiplicative nature of the noise is more evident. The ratio of the variance of the noise in the snowball attractor vs. warm attractor is of the order $((1 - \alpha_{min})/(1 - \alpha_W))^2 \sim 3$. Loosely speaking, the competing warm and snowball climate states have different statistical mechanical, microscopic - as well as thermodynamical, macroscopic - temperatures.

IV. RESULTS

We first treat in detail three cases inside the region of bistability depicted in Fig. 1, namely $\mu = 0.98$ (close to the tipping point $\mu_{W \rightarrow SB}$), $\mu = 1.0$ (corresponding to present-day solar irradiance), and $\mu = 1.02$ (in the parametric region where the M state undergoes a symmetry-break bifurcation). We then construct the weak-noise limit of the invariant measures for all the values of

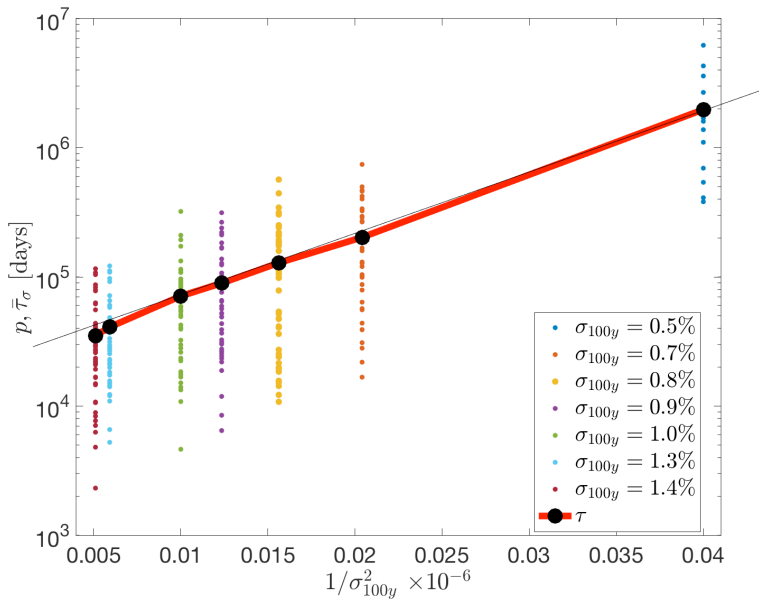


FIG. 2. Statistics of the escape times p for the noise-induced $W \rightarrow SB$ transitions for various noise strengths. Each coloured dot corresponds to an observed escape time p . The estimate of the expected escape times $\bar{\tau}_\sigma$ are indicated by the black dots connected by the red line. The slope of the straight line fit gives the potential difference described in Eq. 5. See [61] for an optimal algorithm for estimating the potential difference.

μ in the region of bistability. We remark that the results shown in Figs. 2, 3, and 5a) have already been reported in the short communication [37], but we deem extremely useful to present them here as well because they are now part of a much more complex, coherent, and detailed narration.

A. Escapes from Basins of Attraction and Instantons

In the case of $\mu = 0.98$, we first perform a set of simulations with noise of different intensity ranging from $\sigma_\tau = 0.5\%$ to $\sigma_\tau = 1.4\%$, with $\tau = 100$ years (y). For each value of the noise intensity, we initialise 50 trajectories in the basin of attraction of the warm climate and study the statistics of the escape time to the snowball attractor. When the transition takes place, we stop the integrations. We observe (not shown) that for each value of σ_τ the escape times are to a good approximation exponentially distributed, thus obeying Eq. 4; the process of transition behaves like a Poisson process. The results on the expectation value of the transition times are presented in Fig. 2, where we show that, indeed, τ_σ agrees with the prediction of Eq. 5. Hence, it is possible

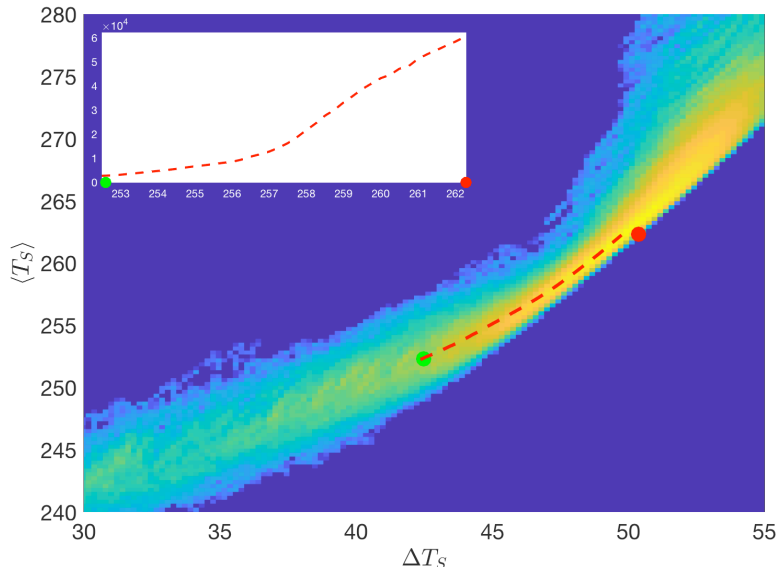


FIG. 3. Main graph: Logarithm of the transient density $\tilde{\rho}$ in the reduced space $(\Delta T_S, \langle T_S \rangle)$, with indication of the actual position of the warm attractor (red dot) and the M state (green dot) for $\mu = 0.98$. We have used $\sigma_{100y} = 1\%$. The $W \rightarrow SB$ approximate instanton is indicated. Top left inset: pdf along the path of the instanton ($\langle T_S \rangle$ on the x-axis).

to define the difference between the value of the pseudo-potential Φ at the M state and at the warm attractor as the slope of the straight line. For reference, we have that for $\sigma_{100y} = 0.5\%$ the average escape time is about $5.2 \times 10^3 y$. We can predict that the escape rate increases to about $1.5 \times 10^7 y$ when $\sigma_{100y} \sim 0.3\%$. We have that the slope of the straight line in Fig. 2 gives $\sim 2(\Phi(M) - \Phi(W))$. Therefore, we show that it is indeed possible to estimate quantitatively the properties of the pseudo-potential also in a very high-dimensional dynamical system like the one considered here. The operation can be repeated for all the other values of μ in the range of multistability and for the processes of escape from the snowball attractor, but we do not pursue here a systematic study of this.

We then wish to look at the paths corresponding to the transitions. Following the discussion in [18, 28], we choose to consider the reduced phase space spanned by the globally averaged surface ocean temperature $\langle T_S \rangle$ and by the meridional temperature difference ΔT_S , defined as the difference between the spatially averaged ocean temperature field between the Equator and $30^\circ N$ and between $30^\circ N$ and the North Pole. This reduced phase space provides a minimal yet physically informative viewpoint on the problem, because it is directly linked with the main physical processes

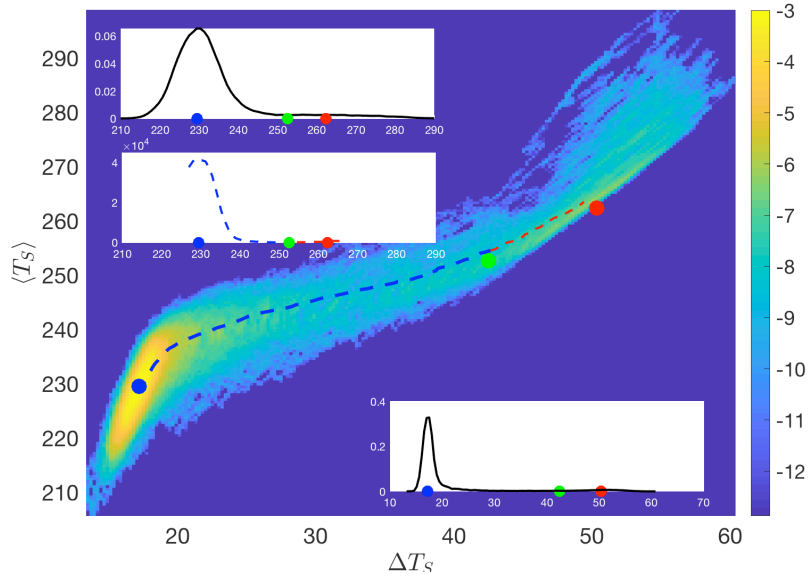


FIG. 4. Main graph: density in the projected phase space $(\Delta T_S, \langle T_S \rangle)$, with indication of the actual position of the warm attractor (red dot), snowball attractor (blue dot), M state (green dot) for $\mu = 0.98$. The $W \rightarrow SB$ and $SB \rightarrow W$ approximate instantons are also indicated. We have used $\sigma_{100y} = 1.5\%$. Top left inset: marginal pdf with respect to $\langle T_S \rangle$. Bottom right inset: marginal pdf with respect to ΔT_S . Center left inset: pdf along the path of the two instantons.

occurring in the climate model:

- The average surface temperature $\langle T_S \rangle$ is directly associated to the positive ice-albedo feedback and the negative Boltzmann radiative feedback;
- The meridional temperature difference ΔT controls the meridional heat transport performed by the ocean, as a result of the diffusive law we insert into its evolution equation,
- The meridional temperature gradient ΔT also controls the meridional heat transport performed by the atmosphere, as a result of the mechanism of baroclinic instability [62].

Figure 3 depicts, for the case $\sigma_\tau = 1.0\%$, the transient two-dimensional distribution function $\tilde{\rho}$ constructed using a frequentist approach using the 50 simulations described above, where the statistics is collected only until the $W \rightarrow SB$ transition is realised. The distribution we obtain cannot be interpreted as an approximation of the invariant measure, because the integrations are stopped after the transitions. Nonetheless, it is apparent that the transitions take prominently place

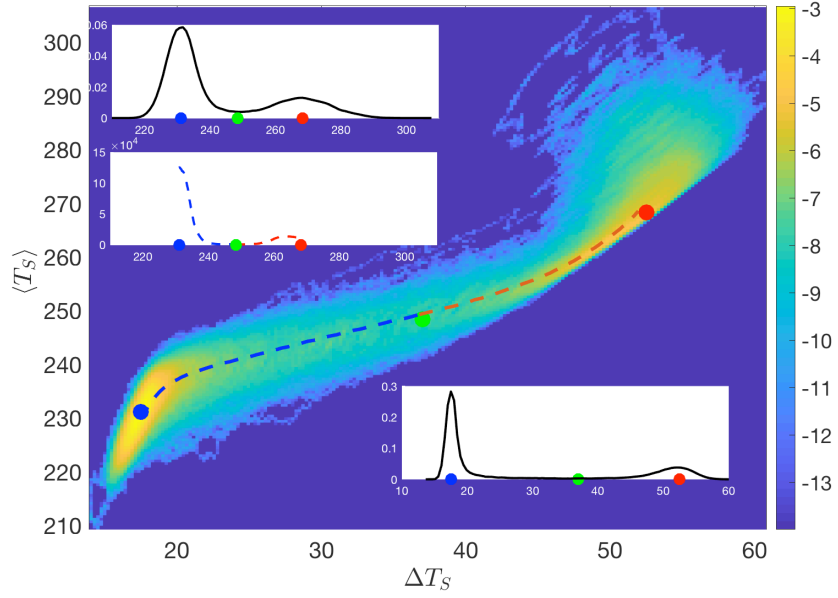
in a very narrow band linking the warm attractor and the M state³. In order to obtain a better understanding of the transition paths, we construct an estimate of the instanton linking the warm attractor to the M state and associated to the $W \rightarrow SB$ transitions by conditionally averaging the trajectories according to the value of $\langle T_S \rangle$. To a good approximation, the instanton connects the warm attractor to the M state, and follows a path of decreasing density. We do not find evidence of different paths for the trajectories leading to an escape and the relaxation trajectories, which is, instead, a typical signature of non-equilibrium [63]. This can be explained by considering [28], where it is shown that the ocean model evolve to a good approximation in an energy landscape. See also Appendix A.

B. Construction of the Invariant Measure

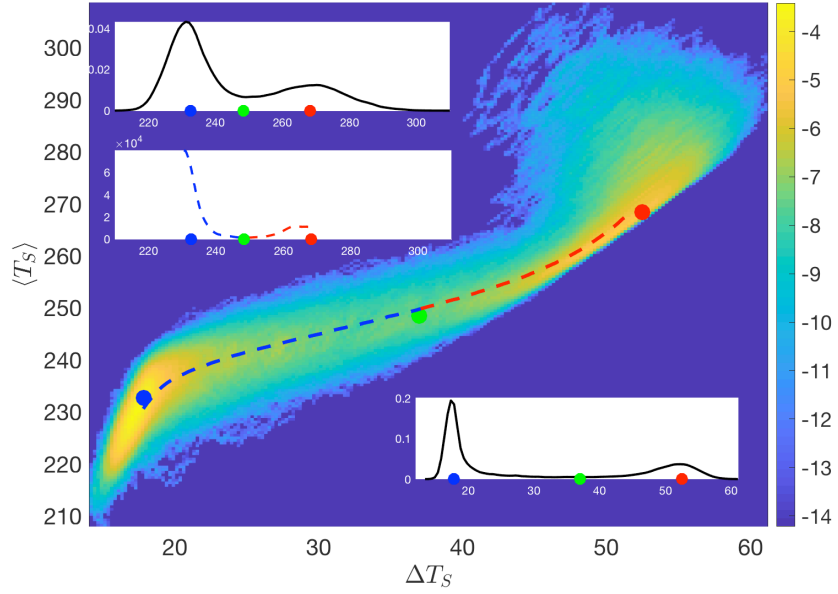
The information contained in Fig. 3 is limited because we are studying only $W \rightarrow SB$ escape processes, and we do not allow for the establishment of an invariant measure. The problem lies in the fact that the pseudo-potential minimum associated to the SB attractor is much deeper than the one associated to the W attractor, so that the average escape time associated to $SB \rightarrow W$ transitions is prohibitively long for the range of (rather weak) noise intensities used for constructing Fig. 3. In fact, in order to be able to construct the invariant measure of the system, we need to observe a sufficient number of $W \rightarrow SB$ and $SB \rightarrow W$ transitions, in order to be sure that we have collected a satisfactory statistics; see also the master equations for the populations given in Eqs. 9-10. We next increase the noise intensity by setting $\sigma_{100y} = 1.8\%$, so that, in an integration lasting about $1.0 \times 10^4 y$, we observe 10 $SB \rightarrow W$ and $W \rightarrow SB$ transitions, The number of transitions is low because it is extremely hard to escape from the SB state.

Our results are shown in Fig. 4. We portray the logarithm of the projection of the invariant measure on the $(\Delta T_S, \langle T_S \rangle)$ plane; we refer to this also as the two-dimensional probability distribution function (pdf). We have that the peaks of the pdf are in good agreement with the position of the W and SB attractors, as implied by the large deviation result presented in Eq. 3. The agreement is even clearer when considering the two marginal pdfs, constructed by projecting the invariant measure on the one dimensional spaces defined by ΔT_S and $\langle T_S \rangle$. Note that the peak over the W state is hardly noticeable because the occupation of the state is extremely low (less than 5% of the

³ Note that, even if the warm attractor and the M state look like dots, they have, in fact, a finite (yet very small) size, because they are both chaotic (see caption of Fig. 1). Here we are considering oceanic variables, which feature a very small variability in the deterministic chaotic case.



a)



b)

FIG. 5. Panel a) Main graph: density in the projected phase space $(\Delta T_S, \langle T_S \rangle)$, with indication of the actual position of the warm attractor (red dot), snowball attractor (blue dot), M state (green dot) for $\mu = 1$. The $W \rightarrow SB$ and $SB \rightarrow W$ approximate instantons are also indicated. We have used $\sigma_{100y} = 1.5\%$. Top left inset: marginal pdf with respect to $\langle T_S \rangle$. Bottom right inset: marginal pdf with respect to ΔT_S . Center left inset: pdf along the path of the two instantons. Panel b) Same as panel a), with $\sigma_{100y} = 1.8\%$.

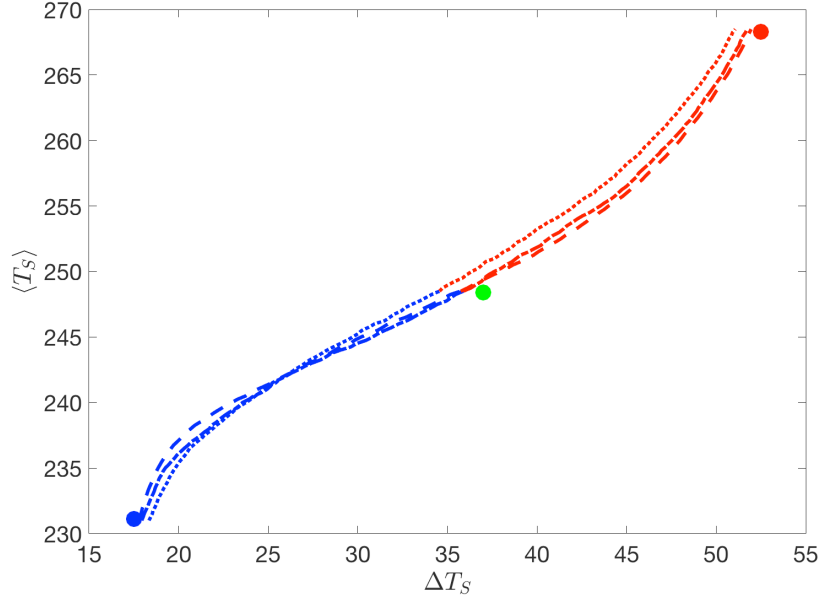


FIG. 6. Estimate of the instantons for $\mu = 1$ obtained using $\sigma_{100y} = 1.5\%$ (dashed lines), $\sigma_{100y} = 1.8\%$ (dash-dotted lines), and $\sigma_{100y} = 2.5\%$ (dotted lines). The red (blue) lines show the estimates for the $W \rightarrow SB$ ($SB \rightarrow W$) instanton. The dots indicate the actual position of the warm attractor (red dot), snowball attractor (blue dot), and M state (green dot). The estimate of the instanton improves as the intensity of the noise is reduced.

total); compare with the cases studied below where higher values of μ are considered. We are also able to construct both the $W \rightarrow SB$ and the $SB \rightarrow W$ instantons, whose starting points agree remarkably well with the position of the W and the SB attractor, respectively, while their final points are in good agreement with the position of the M state. By constructing the pdf along the instantons, we find that they follow a path of monotonic descent (indeed, they follow closely the crests of the pdf), with the minimum located at the M state. Again, this last property can be hardly visualised in Fig. 3 for the $W \rightarrow SB$ instanton (see inset), because the population near the W state is quite small.

Next, we repeat the analysis for $\mu = 1$; results are shown in Figs. 5a)-b). In panel a) we consider an integration with $\sigma_{100y} = 1.5\%$ lasting about $2.9 \times 10^4 y$ and characterised by 41 $SB \rightarrow W$ and $W \rightarrow SB$ transitions. We have an occupation of about 30% for the W basin of attraction, and of about 70% for the SB basin of attraction; additionally, we have $\tau_\sigma^{W \rightarrow SB} \sim 210y$ and $\tau_\sigma^{SB \rightarrow W} \sim 460y$. Also in this case, the projection of the invariant measure in the $(\Delta T_S, \langle T_S \rangle)$

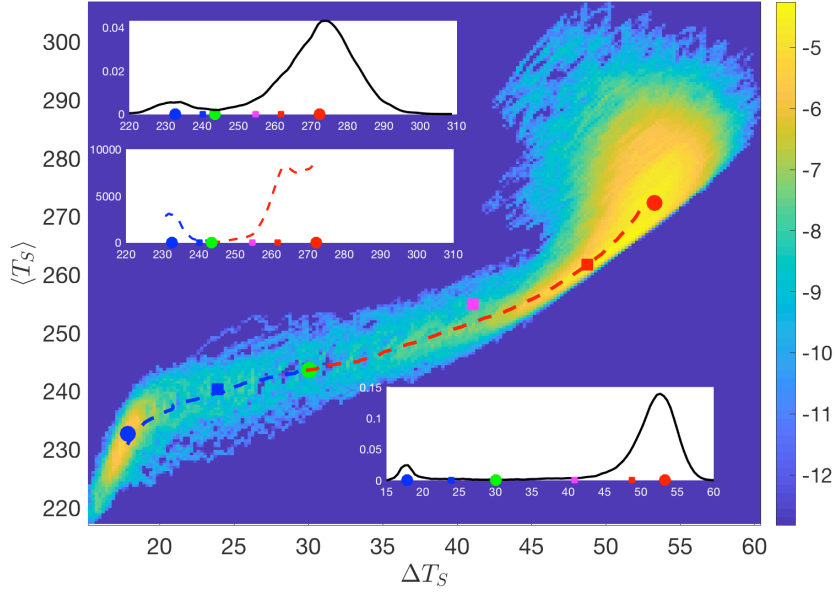


FIG. 7. Main graph: density in the projected phase space $(\Delta T_S, \langle T_S \rangle)$, with indication of the position of the warm attractor (red dot), snowball attractor (blue dot), transient M state (green dot) for $\mu = 1.02$. The squares indicate the properties of the asymptotic M state: warm sector (red square); cold sector (blue square); average (magenta square). The estimates of the $W \rightarrow SB$ and $SB \rightarrow W$ instantons are also indicated as the red and the blue line, respectively. We have used $\sigma_{100y} = 1.5\%$. Top left inset: marginal pdf with respect to $\langle T_S \rangle$. Bottom right inset: marginal pdf with respect to ΔT_S . Center left inset: pdf along the path of the two instantons.

plane shows that there is good agreement between the position of the peaks of the pdfs and the attractors, and that the estimates of the instantons connect attractors and M states with a good precision. It is also clear that the instantons follow a path of descent in terms of probability, as shown by the central inset.

In Panel b) we show the results of repeating the analysis for $\sigma_{100y} = 1.8\%$. In this case the simulation lasts about $2.7 \times 10^4 y$ and we obtain 73 $SB \rightarrow W$ and $W \rightarrow SB$ transitions, and we can draw similar conclusions as in Panel a) regarding the relative position of the attractors, of the M state, and of the instantions. The marginal pdfs are clearly less peaked than in Panel a); the occupancy rate changes slightly with respect to the previous case: it is about 35% for the W basin of attraction, and of about 65% for the SB . Instead, the average escape times change more substantially, and can be estimated as $\tau_\sigma^{W \rightarrow SB} \sim 160y$ and $\tau_\sigma^{SB \rightarrow W} \sim 300y$. These last two

results indicate that the difference between the value of the pseudo-potential at the two competing attractors is relatively small. We will explore this matter in Subsect. IV D, where we will try to deduce where the pseudo-potential reaches its absolute minimum for each value of μ in the bistable region.

It is worth looking more in detail at how the estimate of the instantons is impacted by the intensity of the noise used in the simulation. As instantons are defined in the weak-noise limit, we would expect that one achieves higher precision when weaker noise is used. This is confirmed by the results shown in Fig. 6: we have that the estimates of the instantons obtained using lower noise intensity come closer to the attractors and to the M state. Nonetheless, also the instantons obtained for very strong noise are still relatively accurate.

C. Instantons and Transitions across the Symmetry-broken Melancholia State

We next examine the noise-induced transitions for $\mu = 1.02$. This case is quite interesting because, as discussed in [18] and reported in Fig. 1, the longitudinally-symmetric M state is transient with a very long life time, and slowly evolves into a symmetry broken M state featuring a relatively cold and a relatively warm region, separated by two small regions with large longitudinal temperature gradient at all latitudes. It seems relevant to test whether noise-induced transitions take place through the transient, symmetric M state or the true, symmetry-broken one. Results are shown in Fig. 7, where we use data from a simulation lasting about $10^4 y$ with $\sigma_{100y} = 1.5\%$. We observe only 6 transitions in both directions. This time, as opposed to the case of $\mu = 0.98$, the figure is so low because it is extremely hard to escape from the W state. We estimate the escape times as $\tau_{\sigma}^{W \rightarrow SB} \sim 1400y$ and $\tau_{\sigma}^{SB \rightarrow W} \sim 140y$. We portray the logarithm of the invariant measure of the system in the usual projected space, and the estimates of the instantons. We first observe that in this case most of the density is concentrated around the warm attractor, and a nontrivial relation exists between the paths of the instantons and the dynamical structures on the basin boundary. It is clear that the transient M state plays the role of the gateway of transitions as seen in the previous cases, despite its transient nature. The noise induced transitions do not go through the actual M state (magenta square), while they seem to go thorough states resembling the properties of the warm (red square) and cold (blue square) sectors in the asymptotic M state. This feature might result from the consideration of noise with finite (and not infinitesimal) strength: the pseudo-potential near the transient M state might be just barely higher than that of the asymptotic

M state (and possibly with a more favourable pre-exponential factor), so that a small but finite noise perturbation might push an orbit near the transient M state into the other basin of attraction. Alternatively, this feature might be a subtle signature of dynamical, noise-induced stabilization [55]; this would provide a slight contradiction of our working hypothesis discussed after Eq. 3.

D. Selection of the Limit Measure in the Weak-noise Limit and First-order Phase Transition

Equation 11 indicates that, in the weak-noise limit, all of the measure will be concentrated on the attractor featuring the lowest value for the pseudo-potential Φ . Since for $\mu < S_{W \rightarrow SB}^*/S_0^*$ only the SB state is realised, physical intuition suggests that for low values of μ within the range of bistability, the snowball attractor should contain all the mass in the limit of weak noise, as one can also anticipate by looking at Fig. 3. Conversely, one expects that for high values of μ within the range of bistability, the W should be dominant in the weak noise limit. It is reasonable (yet far from obvious or rigorous) to expect that there should be a critical value of $\mu = \mu_{crit}$ separating the two regimes. Following [18], we consider 18 equally spaced values of μ ($\Delta\mu = 0.005$) within the multistable regime. For each of these values of μ (excluding the case of $\mu = 1.045$, where three stable states are realised) the fraction of the population residing within the basin of attraction of the deterministic warm attractor $P_{W,\sigma}(\mu)$ and its complement, residing in the basin of attraction of the snowball attractor $P_{SB,\sigma}(\mu)$. Related results are shown in Fig. 8. We show how the probability distribution of the variable $\langle T_S \rangle$ depends on μ for three different noise levels: $\sigma_{100y} = 1.5\%$ (Panel a), $\sigma_{100y} = 1.8\%$ (Panel b), and $\sigma_{100y} = 2.5\%$ (Panel c). In these panels we superimpose the bifurcation diagram reported in Fig. 1a). We observe that as the noise is reduced, for all values of μ the distributions are a) more peaked around the attractors; and b) one of the attractors becomes clearly dominant.

In Panel d) the plot for each value of μ the integral of the pdfs reported in the three panels a), b), c) up to the values of $\langle T_S \rangle$ corresponding to the M state (green continuous and dotted lines). To a very good degree of approximation, this corresponds to the integral of the invariant measure over the support of the deterministic basin of attraction of the SB climate. We obtain that for decreasing values of the noise intensity, the emerging invariant measure converges to the deterministic measure supported on the snowball attractor for $\mu \leq \mu_{crit} \approx 1.005$, while the invariant measure converges to the deterministic measure supported on the warm attractor for $\mu \geq \mu_{crit} \approx 1.005$. The absolute minimum of the pseudo-potential Φ is realised in the warm

attractor for $\mu \geq \mu_{crit}$ and in the snowball attractor for $\mu \leq \mu_{crit}$. The changeover is, curiously, quite close to the reference case $\mu = 1$, for which the weak-noise limit of the measure is given by the SB state.

We add a note on the uncertainty associated to the figures reported in Fig. 8d). We remark that for all values of μ and σ we have used simulations lasting at least $10^4 y$. For very low (≤ 0.98) and very large (≥ 1.02) values of μ in the considered range, the simulation length does not allow for observing more than few transitions for the two lowest considered noise level. Therefore, according to the fact that the transitions occur following a Poisson law, one expects in this range an uncertainty on the figures reported in Fig. 8 of the order of the values of the smaller between $P_{SB,\sigma}(\mu)$ and $P_{W,\sigma}(\mu)$. This corresponds, in fact, to a low uncertainty, because most of the mass is concentrated near one of the two deterministic attractors. The uncertainty is quite small for $0.98 \leq \mu \leq 1.03$, because, in all cases, we observe relatively many transitions. The uncertainty in this range can be safely estimated to be below 5%. Summarising, while the values reported in Fig. 8d) might have some non-negligible uncertainties, it seems that the estimate of μ_{crit} is quite robust.

Finally, we have verified that for all values of μ the escape time $\tau_{\sigma}^{W \rightarrow SB}$ and $\tau_{\sigma}^{SB \rightarrow \tau}$ grow rapidly with decreasing values of the intensity of the noise for all values of μ . In agreement with what is shown in Fig. 8, we have that $\tau_{\sigma}^{SB \rightarrow W\tau}$ grows more rapidly than $\tau_{\sigma}^{W \rightarrow SB\tau}$ for $\mu \leq \mu_{crit}$ (and viceversa for $\mu \geq \mu_{crit}$). As a result, in the weak-noise limit an individual trajectory might be trapped for a very long time in the metastable, non-asymptotic state. We remark that we have not performed here a systematic evaluation of the exponential relationship between the escape times and σ , as instead done for $\mu = 0.98$ and shown in Fig. 2, also because, as for the reasons explained before, this would require computational resources that are beyond what has been allocated for this study. We remark that this would allow for evaluating for each value of μ the difference between the value of the pseudo-potential realised at the attractors and at the M state. The algorithm proposed in [61] can be very useful to reduce the computational burden.

We can say that for $\mu = \mu_{crit}$ our system exhibits a behaviour that is reminiscent of a first-order phase transition for near-equilibrium statistical mechanical systems, like a liquid-gaseous transition. In our case, μ is the control parameter (corresponding to the temperature in the equilibrium case), the pseudo-potential Φ is the equivalent of a thermodynamic potential, the scaling factor for the noise intensity σ is the equivalent of (square root of) the temperature, and the globally averaged surface temperature $\langle T_S \rangle$ is the natural order parameter, e.g. density. The discontinuous

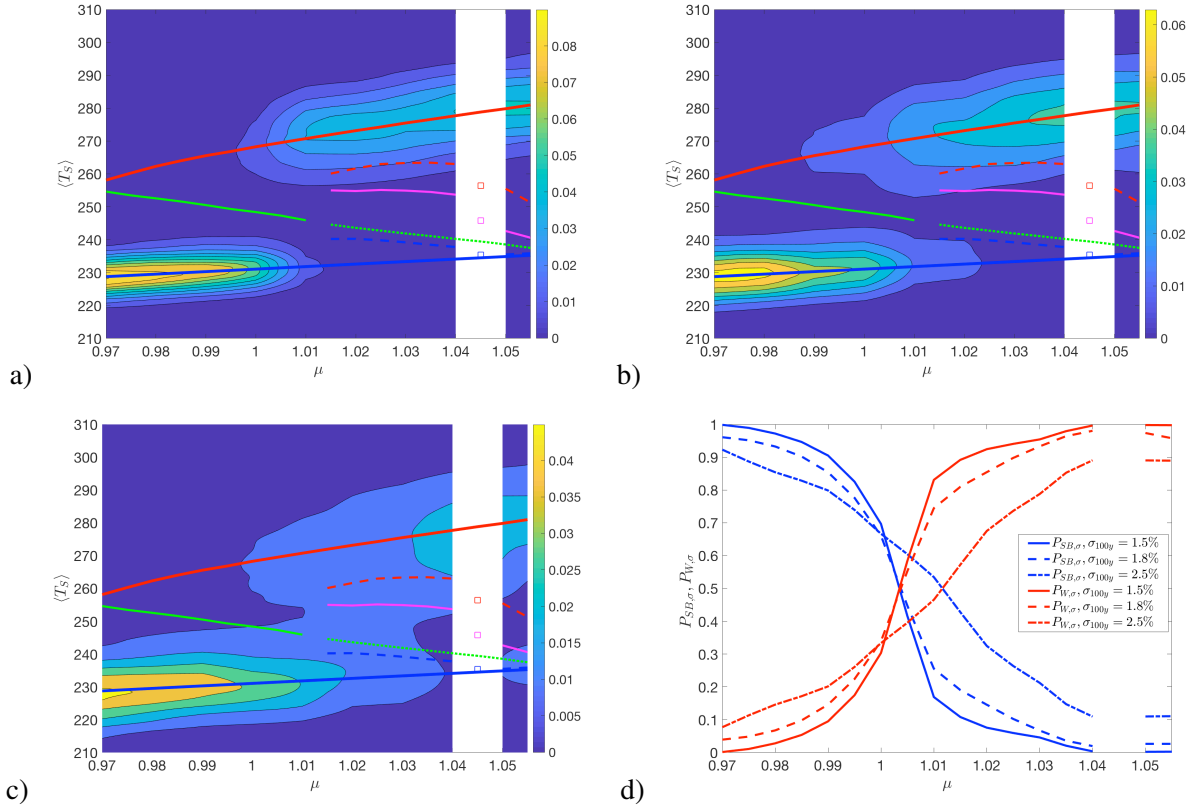


FIG. 8. Projection of the measure on the variable $\langle T_S \rangle$ for $\sigma_{100y} = 1.5\%$ (Panel a), $\sigma_{100y} = 1.8\%$ (Panel b), and $\sigma_{100y} = 2.5\%$ (Panel c). The spacing of the isolines is the same in the three panels. Panel d): Fraction of the measure supported in the basin of attraction of the snowball state as a function of μ and of the noise intensity. As the noise decreases, we observe a fast transition between SB - and W -dominated populations for $\mu = \mu_{crit} \approx 1.005$, which corresponds to a first-order phase transition.

change in the properties of the system for $\mu = \mu_{crit}$ is associated to the change in the amount of absorbed and emitted radiation, as a result of the macroscopic change in the albedo of the planet due to the discontinuity in the position of the ice-line. We remark that choosing a different noise law would in general lead to a different value of μ_{crit} , as a result of the fact that the functional form of Φ would be different.

V. CONCLUSIONS

The goal of this paper has been the investigation of the properties of the noise-induced transitions across the multiple basins of attractions in an intermediate complexity climate model with

$O(10^4)$ degrees of freedom, describing the coupled evolution of atmospheric (fast) and oceanic (slow) variables. The model features the co-existence of warm and snowball attractors for a fairly broad range of values of the solar irradiance. In a previous investigation we had been able to construct the full phase portrait of the deterministic version of the climate model considered here, and had constructed, beside the attractors, the M states of the climate system in the region of bistability [18].

The stochastic forcing is introduced here as a random modulation for the incoming solar radiation, and leads to a nontrivial multiplicative noise law, because the radiative forcing is affected by the albedo of the surface, which, in turn, depends on the surface temperature. The noise, by allowing transitions between the deterministic basins of attraction, allows for establishing an (apparently) ergodic invariant measure of the system. The theory of stochastic differential equations indicates that for systems obeying the hypoellipticity condition, and for a suitable class of noise laws including additive laws and special multiplicative laws like the one considered here, one can write fairly generally the invariant measures in terms of a large deviation law, where the rate function is written as a product of a pseudo-potential and twice the inverse of the parameter controlling the variance of the noise. The pseudo-potential has local minima on the support of the deterministic attractors, and is constant on each of them. In the weak noise limit, transitions take place along special paths called instantons, which link the deterministic attractors and the M states. Such paths are characterised by having minimal cost for an action that is constructed in terms of the deterministic dynamics and of the noise law. While, for a given deterministic dynamics, instantons corresponding to different noise laws follow different paths, they all share the properties of linking the same deterministic attractors to the same M states. This property can be exploited to geometrically construct M states from stochastic simulations, without the need to resort to the edge tracking algorithm; see Appendix A.

We have studied in detail the noise-induced transitions between the deterministic basins of attraction in the range of multistability, extending the results presented in a short communication [37]. We have shown that by studying how the average escape time depends on the intensity of the noise it is possible to estimate the difference between the value of the pseudo-potential at the M state and at the attractor the trajectories are escaping from. The estimates of the instantons are shown to become more precise as we consider simulations where weaker noise is considered. The instanton, in a case of special interest where the M state was shown to undergo a symmetry-break process, selects as optimal point of passage between the snowball and the warm climate the

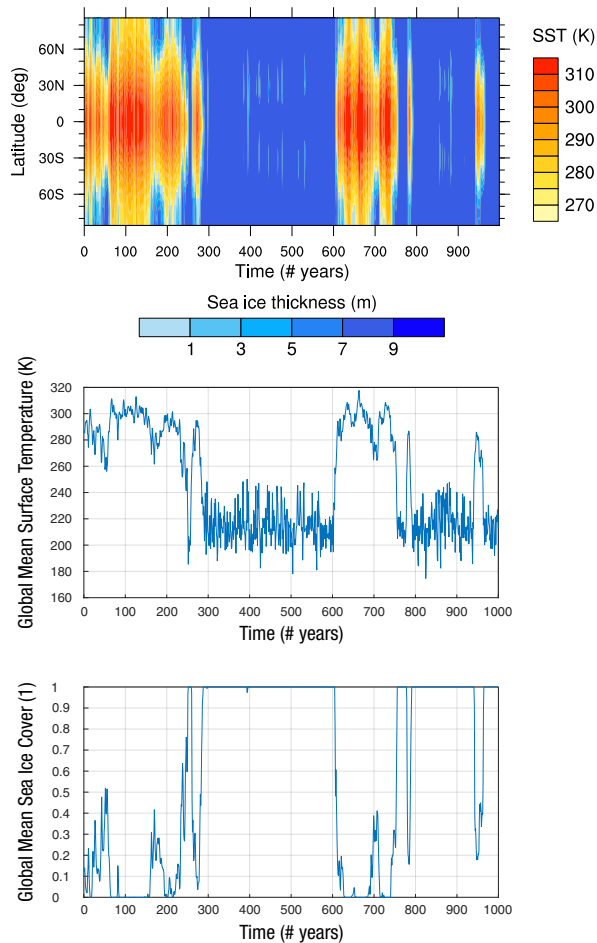


FIG. 9. Example of noise-induced transitions between snowball and warm climate state for present-day solar constant ($\sigma_{100y} = 2\%$) for the climate model PLASIM [64] in a simulation of $10^3 y$. From top to bottom: zonal averages of the temperature field and of the sea ice cover; globally averaged surface temperature; fraction of ice-covered ocean. The characteristic escape times is comparable with what is obtained in the simpler model PUMA-GS used in this work (courtesy of C. Kilic).

transient M state instead of the asymptotic one, possibly as a result of the finite amplitude of the noise, or as a manifestation of noise-driven dynamical stabilisation.

Finally, by studying how the populations of the warm and snowball climate change as a function of the intensity of the noise, and using the large deviation law for the measure predicted by the theory, we find an estimate of a critical value of $\mu = \mu_{crit} \approx 1.005$ such that for $\mu \geq \mu_{crit}$ the zero-noise limit of the invariant measure is supported on the warm deterministic attractor, while for $\mu \leq \mu_{crit}$ the weak noise limit of the invariant measure is supported on the snowball attractor. The

asymptotic state corresponds to the attractor featuring the lowest value of the pseudo-potential.

These results obtained here indicate that, as soon as some form of noise is added into the system, multistability is factually lost in the weak-noise limit, as the noise law is responsible for selecting, for each value of the control parameter (here μ), a specific asymptotic state. Changing the value of the control parameter, one will find one or more abrupt transitions in the statistical properties of the system (here realised at μ_{crit}), i.e., in other terms discontinuities in the response of the system to changes in the control parameter. What happens in our model at $\mu = \mu_{crit}$ is mathematically analogous of a first-order phase transition occurring in a near-equilibrium statistical mechanical system. We remark that, since the escape time away from either attractor grows exponentially with the inverse of the parameter controlling the variance of the noise, an individual trajectory might be trapped for very long time in a metastable state.

In collaboration with C. Kilic (Bern) and F. Lunkeit (Hamburg) the authors have started some preliminary simulations where stochastic forcing is added to PLASIM [64], a much more complex climate model than the one used in this study (yet missing some essential ocean dynamical processes). As shown in Fig. 9, the first results we have obtained are encouraging in indicating that the findings of this paper might be relevant for more realistic model configurations. For the future, we aim at obtaining detailed information on the large scale properties of the flow configurations leading to the noise-induced transitions, taking the thermodynamic lens we originally explored in [9]. The overall goal is to advance our knowledge of the global properties of the climate system by linking its statistical mechanical and its thermodynamical descriptions. An important question of specific relevance for paleoclimatic and planetary science studies is to understand whether the third climatic state found in [18] for $\mu = 1.045$ is recovered also for more complex model configurations.

The approach presented here, based upon combining the knowledge of the dynamical landscape of a multistable deterministic dynamical systems with the analysis of the impacts of stochastic perturbations, seems of more general interest than the specific problem we have studied. We believe that it can be key for addressing the challenge of understanding tipping points in the Earth system [49] as well as providing insights to a large class of multistable systems [48]. We will dedicate future efforts exactly to exploring these research lines, in particularly looking at the Atlantic meridional overturning circulation, an element of the global ocean circulation that is well known to have more than one competing *modes of operation*. The occurrence of one or of the other state has important implications on the global climate, and rather dramatic ones for the regional climate of the

North Atlantic sector; see [65] for a review of this topic. Multistability has been recently reported in the von Karman turbulent flow in [66]: the methods proposed in this paper could elucidate paths and mechanisms underlying the transitions between the asymptotic states.

A. An Interdisciplinary Outlook: Evolutionary Biology

We wish to conclude this paper by reaching out to other scientific disciplines and to a more conceptual level. In the influential book discussing the Cambrian fossils from the Burgess shale and their importance for explaining the mechanisms of evolution, Gould [47] presents some ideas on the scientific methodology inherent to historical sciences, and, specifically, to evolutionary biology. He clarifies that historical scientific explanations take the form of a narrative, whereby subsequent phenomena follow in a specific order⁴: the time-ordering and causal links between such phenomena can be discovered and convincingly explained when multiple, independent sources provide indication for the same historical pattern of change. Gould argues that this method is fundamentally different from the classic - which he calls *stereotypical* - scientific method *à la Galileo* whereby one specific experiment can be repeated in idealised conditions, and the final outcomes of the experiment can be predicted using the fundamental laws of nature. The latter is the - indeed too simplified - version he gives of how *hard sciences* work. An obvious difference between the two methods comes from the fact that certain experiments - like the evolution of the climate and of the biosphere of a specific planet - cannot be repeated. Another difference comes from the fact - Gould argues - that historical processes are dominated by *contingency*: while we observe a specific path of historical development, many others of such paths are indeed compatible with the laws of nature, and could have been realised had the system been forced in a slightly different way in the past. We are able to understand the mechanisms of historical development, but not to predict accurately the specific path. Gould argues that the evolution in our planet could have led to fundamentally different forms of life, had the contingencies been different in the distant past. The existence of our own species is the - a priori very unlikely - result of such contingencies. In general, in systems dominated by contingency, *if we could run again the movie the outcome would be vastly different*. Gould's views on evolution have been criticised by authors, as Conway Morris, proposing that *convergence*, rather than contingency, is the main mechanism of evolution, so that evolution is seen as a - mostly - deterministic path of change, of which nowadays we see the un-

⁴ The related *storyline* approach is being currently proposed for studying weather and climate phenomena [67].

avoidable outcome [68]; see the debate in [69]. Some authors have proposed that both mechanisms are indeed in action, yet dominant at different scales of diversification of the organisms [70].

We argue that Gould's view can be put in the context of the mathematical framework discussed in this paper. Stochastically forced complex systems evolve in a phase space where an individual trajectory corresponds to a historical realisation of the system. The historical realisations, even starting from the same initial condition, can be vastly - even qualitatively - different if the deterministic dynamics supports the existence of multiple attractors, because different realisation can be trapped for very long time in very distant regions of the phase space. As discussed here, stochastic forcing allows for the system to jump across the various basins of attraction, and the mechanism defining the evolution of the trajectory are defined by the differential equations. The predictability of the system, both of the first and second kind in the sense of Lorenz, is finite but non-zero. Finally, we can interpret the M states as the true agents of the contingency discussed by Gould. It is not the presence of a forcing, however strong, that changes radically the future history of the system, but rather the existence of special regions of the phase space - near the M states - where even small perturbations can force two nearby trajectories towards qualitatively different future histories. The scenario proposed by Conway Morris is associated to a scenario where M states are either absent - so that the system is not multistable - or the noise is so weak that the probability of getting close to the an M state is exceedingly low, despite the presence of stochastic perturbations, the system will be (almost) always quite close to a specific deterministic attractor, even *if we could run again the movie*, i.e., run another simulation.

While contingency and qualitative changes dominate the behaviour of the system near the M states, quantitative properties, stated in probabilistic terms as large deviation laws defining probability measures and escape rate, can still be defined and tested. This is the main positive outcome of the mathematical and physical framework outlined in this paper.

ACKNOWLEDGMENTS

VL and TB acknowledge the support received by the EU Horizon2020 projects Blue-Action (grant No. 727852) and CRESCENDO (grant No. 641816). VL acknowledges the support of the DFG SFB/Transregio project TRR181 and of the Royal Society Bilateral UK-Russia Grant. The authors wish to thank T. Tél for inspiring exchanges. VL wishes to thank S. Brusatte for pointing to some fascinating literature on evolutionary biology, X.-M. LI for suggesting the importance

of the hypoellipticity condition, and J. Yorke for great encouragement in the course of several cheerful discussions. This paper has been partly prepared during the Advanced Workshop on *Nonequilibrium Systems in Physics, Geosciences, and Life Sciences* held at ICTP, Trieste, on May 15-24 2018.

Appendix A: An Alternative Construction of the M States using Stochastic Perturbations

As discussed in the paper, the construction of M states for multistable systems is far from being a trivial task, and requires the use of the edge tracking algorithm introduced in [29, 30] and used also by the authors in [18, 28]. We wish to propose here a proof of concept of an alternative procedure for constructing the M state without resorting to such an algorithm, but rather using only direct numerical simulations. The procedure discussed below might be useful in the case the edge tracking algorithm might be hard to implement because of the specifics of the system under investigation, or the presence of similar time scales associated to the instability along and across the basin boundary might make the construction of the M state harder to attain. Alternatively, it can be seen as a way to test the results obtained from the study of the deterministic dynamics.

The idea is to exploit the fact that, as discussed in Section II, under rather general conditions on the noise law, the M state, in the weak noise limit, acts as the gate for noise-induced transitions between the competing attractors. We then propose to proceed as follows. Let's consider the following stochastic differential equations:

$$d\mathbf{x}(t) = \mathbf{F}(\mathbf{x}(t))dt + \sigma \mathbf{s}_k(\mathbf{x})d\mathbf{W}, \quad k = 1, \dots, K. \quad (\text{A1})$$

We consider the possibility of perturbing the deterministic flow with K different noise laws, defined by the K functions $\mathbf{s}_k(\mathbf{x})$. We assume, for simplicity, that the deterministic system defined by $\dot{\mathbf{x}}(t) = \mathbf{F}(\mathbf{x}(t))$ is bistable. We choose such K noise laws so that they obey the hypotheses discussed in Sect. II B⁵.

In the weak noise limit defined by $\sigma \rightarrow 0$, the stochastic dynamics of the corresponding SDEs obey Eqs. 3-5. Clearly, for each noise law the prefactor $Z_k(x)$ and the pseudo-potential $\Phi_k(x)$ will be different. Nonetheless, as discussed above, in all cases $\Phi_k(x)$ has a local minimum (and is constant) on the support of the two deterministic attractors, and it is also constant on the M

⁵ The simplest choice is given by K independent and non-degenerate constant matrices s_k , which amount to considering different additive noise laws with associated independent elliptic diffusions, but, as discussed in the text, a much wider range of options is available.

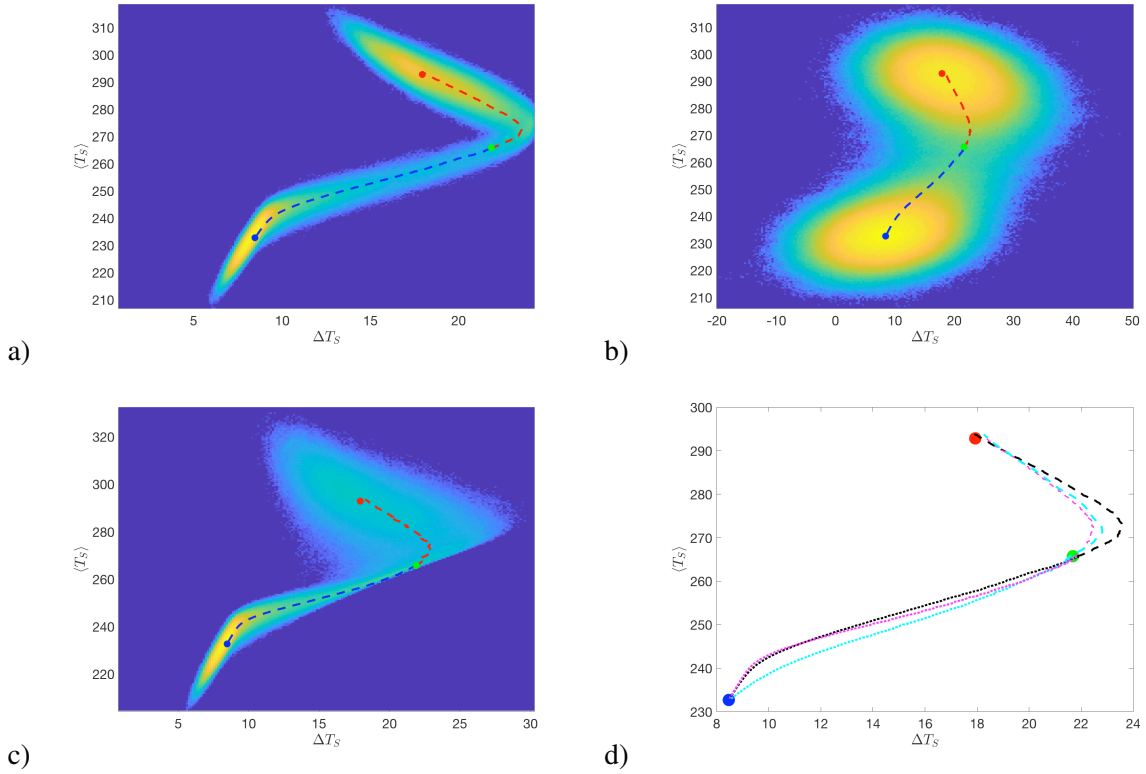


FIG. 10. Projected measure in the $(\Delta T_S, \langle T_S \rangle)$ space for selected stochastically perturbed simulations of the Ghil-Sellers models and related instantons. All results have been obtained with simulations lasting in 1.6×10^6 model years. a) Additive noise s_1 : Logarithm of the pdf, $W \rightarrow SB$ instanton (red dashed line), $SB \rightarrow W$ instanton (blue dashed line); Warm attractor (red dot). SB attractor (blue dot); M state (green dot). The results have been obtained with $\sigma = 0.4$. b) Same as in a), for additive noise s_2 (results obtained setting $\sigma = 2$). c) Same as in a), for the multiplicative noise used in the rest of the paper (results obtained setting $\sigma = 1.0$). d) The instantons from a) (black line), b) (cyan line) and c) (magenta line) are plotted together. Dashed (dotted) lines correspond to the $W \rightarrow SB$ ($SB \rightarrow W$) instantons. They cross at the M state (green dot) and at the warm attractor (red dot) and at the SB attractor (blue dot).

state separating the two attractors. Additionally, while for all values of k the paths defined by the instantons are different (because the Freidlin-Wentzell action depends on the covariance matrix of the noise), they indeed connect the same attractors to the same M state. Assuming that the attractors and the M states are points or at least small sets given in a coarse-grained description of the phase space, we can identify the M state as the only point in space where the instantons of corresponding to all the K noise laws will intersect.

In order to show that this approach does indeed work, we investigate the properties of $K = 3$ variants of the Ghil-Sellers diffusive model we studied in [28], differing for the law of the stochastic perturbation impacting the energy balance of the climate system. The Ghil-Sellers diffusive model can be written by removing the atmosphere-ocean coupling term in Eq. 20. In order to conform to Eq. 2 (note that we treat below the numerical discretization of a stochastically perturbed partial differential equation), we express the three stochastically perturbed models as follows:

$$\frac{\partial T_S(\phi, t)}{\partial t} = \mu \frac{S_0^*}{4} \frac{I(\phi)}{C(\phi)} (1 - \alpha(\phi, T_S)) - \frac{O(T_S)}{C(\phi)} - \frac{D_\phi[T_S]}{C(\phi)} + \sigma s_k(\phi, T_S) \frac{dW}{dt}, \quad k = 1, 2, 3, \quad (\text{A2})$$

where dW is the increment of a one-dimensional Wiener process, and we have:

$$s_1(\phi, T_S) = \mu \frac{S_0^*}{4} \frac{I(\phi)}{C(\phi)}, \quad (\text{A3})$$

$$s_2(\phi, T_S) = 1, \quad (\text{A4})$$

$$s_3(\phi, T_S) = \mu \frac{S_0^*}{4} \frac{I(\phi)}{C(\phi)}, (1 - \alpha(\phi, T_S)). \quad (\text{A5})$$

Specifically, we have that $s_1(\phi, T_S) = s_1(\phi)$ and $s_2(\phi, T_S) = s_2(\phi)$ correspond to additive noise laws, which feature different diffusion matrices. Instead, $s_3(\phi, T_S)$ is a multiplicative noise law as a result of the temperature-dependence of the albedo and is closely related to what was studied in the rest of the paper; see Eq. 20. We construct for these three SDEs the invariant measure and, by stochastically averaging, we estimate the instantons connecting the attractors and the M states. We make sure that these are estimated using very weak noise amplitudes. Results are presented in Fig. 10, where we show the projections on the $(\Delta T_S, \langle T_S \rangle)$ space. Panels a), b), and c) show the invariant measures and the instantons constructed for the noise laws s_1 (using $\sigma = 0.4$), s_2 (using $\sigma = 2.0$), and s_3 (using $\sigma = 1.0$), respectively. Note that the instanton constructed with the multiplicative noise law looks qualitatively different from what is shown in Fig. 5-6, as a result of the lack of atmospheric motions in the simpler model discussed here. Panel d) portrays in the same panels the instantons constructed for the three noise laws. Indeed, we have a confirmation that all of them are different, as a result of the different noise laws of the three SDEs, and intersect at the attractors and at the M state. The position of the M state in the projected phase space can be identified through this geometric procedure, without resorting to the edge tracking method. Considering additional noise laws can be helpful for resolving possible geometrical degeneracies due to the use of a projection. Projecting in dimension higher than 2 could also serve a similar scope.

-
- [1] M.I. Budyko. The effect of solar radiation variations on the climate of the earth. *Tellus*, 21:611–619, 1969.
- [2] WD Sellers. A global climatic model based on the energy balance of the earth-atmosphere system. *J. Appl. Meteorol.*, 8:392–400, 1969.
- [3] M. Ghil. Climate stability for a Sellers-type model. *J. Atmos. Sci.*, 33:3–20, 1976.
- [4] J. L. Kirschvink. Late Proterozoic low-latitude global glaciation: The snowball Earth. In J. W. Schopf and C. Klein, editors, *The Proterozoic Biosphere: A Multidisciplinary Study*, chapter 8, pages 91–92. Cambridge University Press, 1992.
- [5] Paul F. Hoffman and Daniel P. Schrag. The snowball Earth hypothesis: testing the limits of global change. *Terra Nova*, 14(3):129–155, 2002.
- [6] R.T. Pierrehumbert, D.S. Abbot, Aiko Voigt, and D. Koll. Climate of the Neoproterozoic. *Annual Review of Earth and Planetary Sciences*, 39(1):417–460, 2011.
- [7] William T. Hyde, Thomas J. Crowley, Steven K. Baum, and W. Richard Peltier. Neoproterozoic snowball earth simulations with a coupled climate/ice-sheet model. *Nature*, 405:425–429, 2000.
- [8] Aiko Voigt and Jochem Marotzke. The transition from the present-day climate to a modern Snowball Earth. *Climate Dynamics*, 35(5):887–905, 2010.
- [9] Valerio Lucarini, Klaus Fraedrich, and Frank Lunkeit. Thermodynamic analysis of snowball earth hysteresis experiment: Efficiency, entropy production and irreversibility. *Quarterly Journal of the Royal Meteorological Society*, 136(646):2–11, 2010.
- [10] R. Boschi, V. Lucarini, and S. Pascale. Bistability of the climate around the habitable zone: a thermodynamic investigation. *Icarus*, 227:1724–1742, 2013.
- [11] Thomas J. Crowley, William T. Hyde, and W. Richard Peltier. CO₂ levels required for deglaciation of a near-snowball earth. *Geophysical Research Letters*, 28(2):283–286, 2001.
- [12] Manuel Linsenmeier, Salvatore Pascale, and Valerio Lucarini. Climate of earth-like planets with high obliquity and eccentric orbits: Implications for habitability conditions. *Planetary and Space Science*, 105:43 – 59, 2015.
- [13] C. Kilic, C. C. Raible, and T. F. Stocker. Multiple climate states of habitable exoplanets: The role of obliquity and irradiance. *The Astrophysical Journal*, 844(2):147, 2017.
- [14] V Lucarini, S Pascale, R Boschi, E Kirk, and N Iro. Habitability and multistability in earth-like

- plantets. *Astr. Nach.*, 334(6):576–588, 2013.
- [15] Jade Checlair, Kristen Menou, and Dorian S. Abbot. No snowball on habitable tidally locked planets. *The Astrophysical Journal*, 845(2):132, 2017.
- [16] J. P. Lewis, A. J. Weaver, and M. Eby. Snowball versus slushball earth: Dynamic versus nondynamic sea ice? *Journal of Geophysical Research: Oceans*, 112(C11):C11014, 2007.
- [17] Dorian S. Abbot, Aiko Voigt, and Daniel Koll. The jormungand global climate state and implications for neoproterozoic glaciations. *Journal of Geophysical Research: Atmospheres*, 116(D18), 2011.
- [18] Valerio Lucarini and Tamás Bódai. Edge states in the climate system: exploring global instabilities and critical transitions. *Nonlinearity*, 30(7):R32, 2017.
- [19] James F. Kasting, Daniel P. Whitmire, and Ray T. Reynolds. Habitable zones around main sequence stars. *Icarus*, 101(1):108 – 128, 1993.
- [20] Ileana Gómez-Leal, Lisa Kaltenecker, Valerio Lucarini, and Frank Lunkeit. Climate sensitivity to carbon dioxide and the moist greenhouse threshold of earth-like planets under an increasing solar forcing. *The Astrophysical Journal*, 869(2):129, dec 2018.
- [21] Ileana Gómez-Leal, Lisa Kaltenecker, Valerio Lucarini, and Frank Lunkeit. Climate sensitivity to ozone and its relevance on the habitability of earth-like planets. *Icarus*, 321:608 – 618, 2019.
- [22] Viviane Baladi. *Positive Transfer Operators and Decay of Correlations*. World Scientific, Singapore, 2000.
- [23] Mark Pollicott. On the rate of mixing of Axiom A flows. *Inventiones Mathematicae*, 81(3):413–426, October 1985.
- [24] David Ruelle. Resonances of Chaotic Dynamical Systems. *Physical review letters*, 56(5):405–407, 1986.
- [25] Alexis Tantet, Valerio Lucarini, Frank Lunkeit, and Henk A Dijkstra. Crisis of the chaotic attractor of a climate model: a transfer operator approach. *Nonlinearity*, 31(5):2221, 2018.
- [26] Mickaël David Chekroun, J. David Neelin, Dmitri Kondrashov, J. C. McWilliams, and Michael Ghil. Rough parameter dependence in climate models and the role of Ruelle-Pollicott resonances. *Proceedings of the National Academy of Sciences of the United States of America*, 111(5):1684–1690, March 2014.
- [27] Valerio Lucarini. Response operators for markov processes in a finite state space: Radius of convergence and link to the response theory for axiom a systems. *Journal of Statistical Physics*, 162(2):312–333, Jan 2016.

- [28] Tamás Bódai, Valerio Lucarini, Frank Lunkeit, and Robert Boschi. Global instability in the ghil-sellers model. *Clim. Dyn.*, 44(11):3361–3381, 2014.
- [29] Joseph D. Skufca, James A. Yorke, and Bruno Eckhardt. Edge of chaos in a parallel shear flow. *Phys. Rev. Lett.*, 96:174101, May 2006.
- [30] Tobias M. Schneider, Bruno Eckhardt, and James A. Yorke. Turbulence transition and the edge of chaos in pipe flow. *Phys. Rev. Lett.*, 99:034502, Jul 2007.
- [31] Celso Grebogi, Edward Ott, and James A. Yorke. Fractal basin boundaries, long-lived chaotic transients, and unstable-unstable pair bifurcation. *Phys. Rev. Lett.*, 50:935–938, Mar 1983.
- [32] Carl Robert, Kathleen T. Alligood, Edward Ott, and James A. Yorke. Explosions of chaotic sets. *Physica D: Nonlinear Phenomena*, 144(1):44 – 61, 2000.
- [33] E. Ott. *Chaos in Dynamical Systems*. Cambridge University Press, 2002.
- [34] Y.-C. Lai and T. Tél. *Transient Chaos*. Springer, New York, 2011.
- [35] Daniel M. Abrams and Steven H. Strogatz. Chimera states for coupled oscillators. *Phys. Rev. Lett.*, 93:174102, Oct 2004.
- [36] O. E. Omel’chenko. The mathematics behind chimera states. *Nonlinearity*, 31(5):R121, 2018.
- [37] V. Lucarini and T. Bodai. Transitions across Melancholia States in a Climate Model: Reconciling the Deterministic and Stochastic Points of View. *ArXiv e-prints*, August 2018.
- [38] Denis R. Bell. *Stochastic Differential Equations and Hypoelliptic Operators*, pages 9–42. Birkhäuser Boston, Boston, MA, 2004.
- [39] Peter Hanggi. Escape from a metastable state. *Journal of Statistical Physics*, 42(1):105–148, Jan 1986.
- [40] R.L. Kautz. Activation energy for thermally induced escape from a basin of attraction. *Physics Letters A*, 125(6):315 – 319, 1987.
- [41] P Grassberger. Noise-induced escape from attractors. *Journal of Physics A: Mathematical and General*, 22(16):3283, 1989.
- [42] M. I. Freidlin and A.D. Wentzell. *Random Perturbations of Dynamical Systems*. Springer, New York, 1984.
- [43] R. Graham, A. Hamm, and T. Tél. Nonequilibrium potentials for dynamical systems with fractal attractors or repellers. *Phys. Rev. Lett.*, 66:3089–3092, Jun 1991.
- [44] A. Hamm, T. Tél, and R. Graham. Noise-induced attractor explosions near tangent bifurcations. *Physics Letters A*, 185(3):313 – 320, 1994.

- [45] Suso Kraut and Ulrike Feudel. Multistability, noise, and attractor hopping: The crucial role of chaotic saddles. *Phys. Rev. E*, 66:015207, Jul 2002.
- [46] S. Beri, R. Mannella, D. G. Luchinsky, A. N. Silchenko, and P. V. E. McClintock. Solution of the boundary value problem for optimal escape in continuous stochastic systems and maps. *Phys. Rev. E*, 72:036131, Sep 2005.
- [47] S. J. Gould. *Wonderful Life: The Burgess shale and the Nature of History*. W.W. Norton, New York, 1989.
- [48] Ulrike Feudel, Alexander N. Pisarchik, and Kenneth Showalter. Multistability and tipping: From mathematics and physics to climate and brainminireview and preface to the focus issue. *Chaos: An Interdisciplinary Journal of Nonlinear Science*, 28(3):033501, 2018.
- [49] Timothy M. Lenton, Hermann Held, Elmar Kriegler, Jim W. Hall, Wolfgang Lucht, Stefan Rahmstorf, and Hans Joachim Schellnhuber. Tipping elements in the earth’s climate system. *Proceedings of the National Academy of Sciences*, 105(6):1786–1793, 2008.
- [50] F. Brauer and J. A. Nohel. *The Qualitative Theory of Ordinary Differential Equations: An Introduction*. Dover, New York, 1989.
- [51] Juergen Vollmer, Tobias M Schneider, and Bruno Eckhardt. Basin boundary, edge of chaos and edge state in a two-dimensional model. *New Journal of Physics*, 11(1):013040, 2009.
- [52] E. N. Lorenz. The physical bases of climate and climate modelling. climate predictability. In *GARP Publication Series*, pages 132–136. WMO, 1975.
- [53] Brandon S. Lindley and Ira B. Schwartz. An iterative action minimizing method for computing optimal paths in stochastic dynamical systems. *Physica D: Nonlinear Phenomena*, 255:22 – 30, 2013.
- [54] Ying Tang, Ruoshi Yuan, Gaowei Wang, Xiaomei Zhu, and Ping Ao. Potential landscape of high dimensional nonlinear stochastic dynamics with large noise. *Scientific Reports*, 7(1):15762, 2017.
- [55] Ludwig Arnold. *Random Dynamical Systems*. Springer, Berlin, 2003.
- [56] H.A. Kramers. Brownian motion in a field of force and the diffusion model of chemical reactions. *Physica*, 7(4):284 – 304, 1940.
- [57] Thomas Frisius, Frank Lunkeit, Klaus Fraedrich, and Ian N. James. Storm-track organization and variability in a simplified atmospheric global circulation model. *Quarterly Journal of the Royal Meteorological Society*, 124(548):1019–1043, 1998.
- [58] Barry Saltzman. *Dynamical Paleoclimatology*. Academic Press, New York, 2001.
- [59] Jos P Peixoto and Abraham H Oort. *Physics of Climate*. American Institute of Physics, 1992.

- [60] Valerio Lucarini, Richard Blender, Corentin Herbert, Francesco Ragone, Salvatore Pascale, and Jeroen Wouters. Mathematical and Physical Ideas for Climate Science. *Reviews of Geophysics*, 52(4):1 – 51, 2014.
- [61] T. Bódai. An efficient algorithm to estimate the potential barrier height from noise-induced escape time data. *ArXiv e-prints*, August 2018.
- [62] James R. Holton. *An introduction to dynamic meteorology*. International Geophysics Series. Elsevier Academic Press., Burlington, MA, 4 edition, 2004.
- [63] J. Zinn-Justin. *Quantum Field Theory and Critical Phenomena*. Oxford University Press, Oxford, 1996.
- [64] Klaus Fraedrich, Heiko Jansen, Edilbert Kirk, Ute Luksch, and Frank Lunkeit. The Planet Simulator: Towards a user friendly model. *Meteorologische Zeitschrift*, 14(3):299–304, 2005.
- [65] T Kuhlbrodt, A Griesel, M Montoya, A Levermann, M Hofmann, and S Rahmstorf. On the driving processes of the Atlantic meridional overturning circulation. *Atlantic*, 45(2004):RG2001, 2007.
- [66] D. Faranda, Y. Sato, B. Saint-Michel, C. Wiertel, V. Padilla, B. Dubrulle, and F. Daviaud. Stochastic chaos in a turbulent swirling flow. *Phys. Rev. Lett.*, 119:014502, Jul 2017.
- [67] Theodore G. Shepherd, Emily Boyd, Raphael A. Calel, Sandra C. Chapman, Suraje Dessai, Ioana M. Dima-West, Hayley J. Fowler, Rachel James, Douglas Maraun, Olivia Martius, Catherine A. Senior, Adam H. Sobel, David A. Stainforth, Simon F. B. Tett, Kevin E. Trenberth, Bart J. J. M. van den Hurk, Nicholas W. Watkins, Robert L. Wilby, and Dimitri A. Zenghelis. Storylines: an alternative approach to representing uncertainty in physical aspects of climate change. *Climatic Change*, 151(3):555–571, Dec 2018.
- [68] S. Conway Morris. *The crucible of creation: the Burgess Shale and the rise of animals*. Oxford University Press, Oxford, 1998.
- [69] Simon Conway Morris and Stephen Jay Gould. Showdown on the burgess shale. *Natural History magazine*, 107(10):48–55, 1998.
- [70] J. B. Losos. *Improbable destinies: Fate, chance, and the future of evolution*. Riverhead Books, New York, 2017.